CHIN KER YIN

B.Sc.(Hons) Chemistry

2026

SYNTHESIS, CHARACTERIZATION, AND CONFORMATIONAL STUDY OF *N*-ACYLHYDRAZONE DERIVATIVES BEARING AN INDOLE MOIETY

CHIN KER YIN

BACHELOR OF SCIENCE (HONOURS) CHEMISTRY

FACULTY OF SCIENCE

UNIVERSITI TUNKU ABDUL RAHMAN

JUNE 2026

SYNTHESIS, CHARACTERIZATION, AND CONFORMATIONAL STUDY OF *N*-ACYLHYDRAZONE DERIVATIVES BEARING AN INDOLE MOIETY

By

CHIN KER YIN

A Final Year Project report submitted to the Department of

Chemical Science, Faculty of Science,

Universiti Tunku Abdul Rahman,

In partial fulfilment of the requirement for the degree of

Bachelor of Science (Honours) Chemistry

June 2026

ABSTRACT

SYNTHESIS, CHARACTERIZATION, AND CONFORMATIONAL STUDY OF *N*-ACYLHYDRAZONE DERIVATIVES BEARING AN INDOLE MOIETY

Chin Ker Yin

A series of *N*-acylhydrazone derivatives bearing an indole moiety (**SB 1 - SB 10**) were successfully synthesized, with yields ranging from 67% to 96%. In this project, carboxylic acid hydrazide was used as the starting material for the synthesis of *N*-acylhydrazones. A total of ten *N*-acylhydrazones were synthesized through the condensation reactions between the carboxylic acid hydrazide and various benzaldehydes bearing different substituents at different positions. The structures of the carboxylic acid hydrazide and the synthesized *N*-acylhydrazones were characterized by melting-point analysis and spectroscopic techniques, including FTIR, ^{1}H NMR, ^{13}C NMR, DEPT-135, NOE, HMQC, and HMBC.

Based on the relative configuration of the imine (C=N) double bond and the conformation of the amide [C(=O)–NH] bond, the C=N double bonds of the *N*-acylhydrazones were assigned the *E* configuration as confirmed by using NOE experiments. The NOE results indicated that all *N*-acylhydrazones exist as the *E* geometrical isomer. Furthermore, the ^{1}H and ^{13}C NMR spectra of the synthesized *N*-acylhydrazones revealed the presence of *syn*/*anti* conformers arising from the restricted rotation about the [C(=O)–NH] bond. The proportions of the *syn* and *anti* conformers were found in the range of 40% to 68%, respectively, as determined through the integration of the [C(=O)–NH] proton signals in the ^{1}H NMR.

Dynamic NMR experiments indicated that the coalescence temperatures (T_c) for the [C(=O)–NH] signals were in the range of K, while the rotational energy barriers of the *syn/anti* conformers were determined to be between 7 and 77 kJ/mol.

Keywords: Benzaldehyde, Hydrazide, Hydrazone, Indole, NMR

Subject Area: QD241-441 Organic Chemistry

ACKNOWLEDGEMENT

The completion of this research would not have been possible without the support and assistance of many individuals, whose contributions are sincerely appreciated and gratefully acknowledged. First and foremost, I would like to express my sincere gratitude to my supervisor, Dr. Sim Kooi Mow, for his invaluable guidance, continuous support, and constructive advice throughout this project. He consistently conveyed a spirit of intellectual challenge in research and enthusiasm in teaching. Without his guidance and persistent assistance, this report would not have been successfully completed. It has been a great privilege to learn under Dr. Sim, whom I regard as an expert in his field.

I am also deeply thankful to the laboratory officers and assistants for their technical assistance and support, without which the completion of this project would not have proceeded as smoothly.

I would also like to express my heartfelt gratitude to my friends, especially Teoh Kai Xin, for their emotional support throughout this project. In particular, I am deeply grateful to my senior, Charles Lee Kuok Sui, who consistently

encouraged and motivated me and generously shared his knowledge and experience, which were of immense help to me, as well as to senior Yong Jing Yi, for his valuable sharing and advice.

My deepest gratitude also goes to my family for their encouragement, unconditional love, patience, support, and understanding throughout this journey. I am truly thankful for the constant presence, for always being willing to listen, and for standing by me during difficult times. The encouragement and understanding have given me strength, especially during moments of stress and anxiety, and have been a constant source of motivation that has carried me through this project.

DECLARATION

I hereby declare that this final year project report is based on my original work, except for quotations and citations, which have been appropriately acknowledged. I also declare that this report has not been previously or concurrently submitted for any other degree at UTAR or any other institution.

_____

(CHIN KER YIN)

APPROVAL SHEET

This final year project report, entitled "**SYNTHESIS, CHARACTERIZATION, AND CONFORMATIONAL STUDY OF *N*-ACYLHYDRAZONE DERIVATIVES BEARING AN INDOLE MOIETY**" was completed by **CHIN KER YIN** and submitted as partial fulfilment of the requirements for the degree of Bachelor of Science (Honours) Chemistry at Universiti Tunku Abdul Rahman.

Approved by:

_____

(Associate Professor Dr. Sim Kooi Mow) Date: 21 May 2026

Supervisor

Department of Chemical Science

Faculty of Science

Universiti Tunku Abdul Rahman

FACULTY OF SCIENCE

UNIVERSITI TUNKU ABDUL RAHMAN

Date: 21 May 2026

PERMISSION SHEET

It is hereby certified that **CHIN KER YIN** (ID No: **23ADB01328**) has completed this thesis entitled "**SYNTHESIS, CHARACTERIZATION, AND CONFORMATIONAL STUDY OF *N*-ACYLHYDRAZONE DERIVATIVES BEARING AN INDOLE MOIETY**" under the supervision of Associate Professor Dr. Sim Kooi Mow from the Department of Chemical Science, Faculty of Science.

I hereby give permission to the University to upload the softcopy of my final year project report in PDF format into the UTAR Institutional Repository, which may be made accessible to the UTAR community and public.

Yours truly,

(CHIN KER YIN)

FACULTY OF SCIENCE

UNIVERSITI TUNKU ABDUL RAHMAN

COPYRIGHT STATEMENT

This **Final Year Project Report** is submitted in partial fulfilment of the requirements for the degree of **BACHELOR of SCIENCE (HONOURS) CHEMISTRY** at Universiti Tunku Abdul Rahman (UTAR). This **Final Year Project Report** represents the work of the author, except where due acknowledgement has been made in the text. No part of this **Final Year Project** may be reproduced, stored, or transmitted in any form or by any means, whether electronic, mechanical, photocopying, recording, or otherwise, without the prior written permission of the author or UTAR, in accordance with UTAR's Intellectual Property Policy.

TABLE OF CONTENTS

LIST OF TABLES

LIST OF FIGURES

LIST OF SCHEMES

LIST OF SYMBOLS AND ABBREVIATIONS

g/mol	Gram per mole
mmol	Millimole
μM	Micromolar
NAH	*N*-acylhydrazone
TLC	Thin Layer Chromatography
R_f	Retardation factor
ABTS	2,2'-Azinobis(3-ethylbenzothiazoline-6-sulfonicacid)
DPPH	2,2-Diphenyl-1-picrylhydrazyl
FTIR	Fourier Transform Infrared Spectroscopy
nm	Wavelength
NMR	Nuclear Magnetic Resonance
DEPT	Distortionless Enhancement by Polarization Transfer
HMBC	Heteronuclear Multiple Quantum Correlation
HMQC	Heteronuclear Multiple Bond Correlation
NOE	Nuclear Overhauser Effect
Hz	Hertz
J	Coupling constant

s	Singlet
d	Doublet
t	Triplet
dd	Doublet of doublets
m	Multiplet
td	Triplet of doublets
δ	Chemical shift
δ_H	Chemical shift of proton
δ_C	Chemical shift of carbon
T_c	Coalescence temperature
$\Delta\nu$	Peak separation
k_c	Rate constant of *syn/anti* equilibrium
$\Delta G^{\neq}$	Energy of rotational barrier
kJ/mol	Kilojoule per mole

CHAPTER 1

INTRODUCTION

1.1 Indole

Indole (**Figure 1.1**), commonly referred to as benzopyrrole, is an organic compound that has a heterocyclic structure. Its molecular formula is C_8H_7N with a molecular weight of 117.148 g/mol. In its pure form, it is a colorless solid and has a melting point of 52-53 °C. Naturally, indole is found in coal tar and was first studied through indigo, a dye that can be converted into isatin and then into oxindole. Additionally, indole can be produced through a reaction between phenylhydrazine and pyruvic acid (Mathada *et al*., 2021). Moreover, indole is a flat, bicyclic structure where a benzene ring is fused to the nitrogen-containing pyrrole ring at the 2 and 3 positions. This structure contains a total of 10 π-electrons with 8 coming from double bonds and 2 from nitrogen's lone pair. The presence of these electrons indicates that indole is aromatic. The delocalization of these excess π-electrons enhances the reactivity of indole, making it prone to electrophilic substitution reactions. Indoles exhibit strong reaction with acids because to their relatively low basicity, similar to pyrrole. Molecular orbital

analysis indicated that the highest electron density is at the 3-position, which makes it the susceptible to substitution (Sravanthi and Manju, 2016).

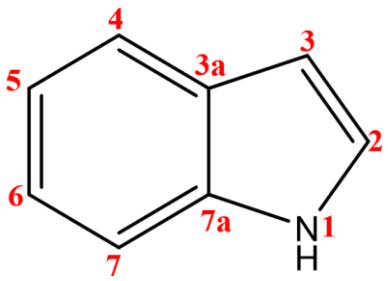

Figure 1.1: Chemical structure of Indole

1.1.1 Application of Indole

Generally, heterocycles are important in chemistry, particularly in areas like drug discovery, photochemistry, agrochemicals, and dye production. Additionally, indole-based structures are integral to the design of several synthetic drugs, forming the core of many therapeutic agents. These privileged structures, such as indole, exhibit strong binding affinities for a variety of receptors, making them valuable for the design of biologically active compounds. Within the indole family, 2-arylindoles stand out as promising drug candidates, showing some bioactivity, such as antibacterial, anticancer, antioxidant, anti-diabetic, anti-inflammatory, antiproliferative, antiviral, and antituberculosis properties (Gautam *et al*., 2024).

1.1.1.2 Anti-Inflammatory Activity

Fever, pain, and inflammation are effectively alleviated by Indomethacin (**Figure 1.2**), which is a nonsteroidal anti-inflammatory drug (NSAID) with an indole structure (Mo *et al*., 2024). For example, NSAIDs are used to treat migraines and headaches, leading to the discovery of headache disorders. Although NSAIDs can easily cross the blood-brain barrier, their high protein binding limits the amount of brain entry. Indomethacin, in particular exhibits stronger vasoconstrictive effects and possesses inhibitory actions through direct neuronal pathways or nitric oxide-dependent mechanisms (Lucas, 2016).

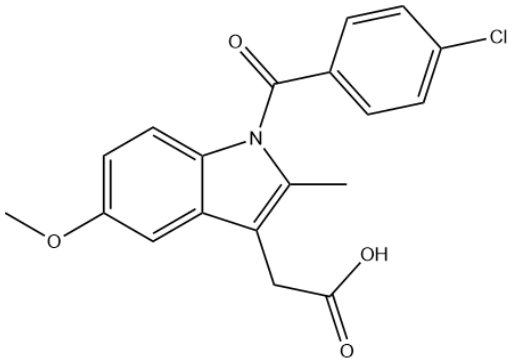

Figure 1.2: Chemical structure of Indometacin

1.1.1.3 Anti-tumour Activity

Vinblastine and Vincristine (**Figure 1.3**) are the first recognized anti-tumor agent which introduced when 1965, known for their ability to inhibit polymerization of tubulin. Vincristine is commonly used in the treatment of acute lymphoblastic

leukemia, as well as Hodgkin's and non-Hodgkin lymphoma. Vinblastine, on the other hand, is mainly prescribed for advanced Hodgkin's disease and germ cell cancer of the testes. Newer vinca alkaloids have been developed to reduce cytotoxicity and enhance efficacy compared to the original compounds (Kaushik *et al*., 2013).

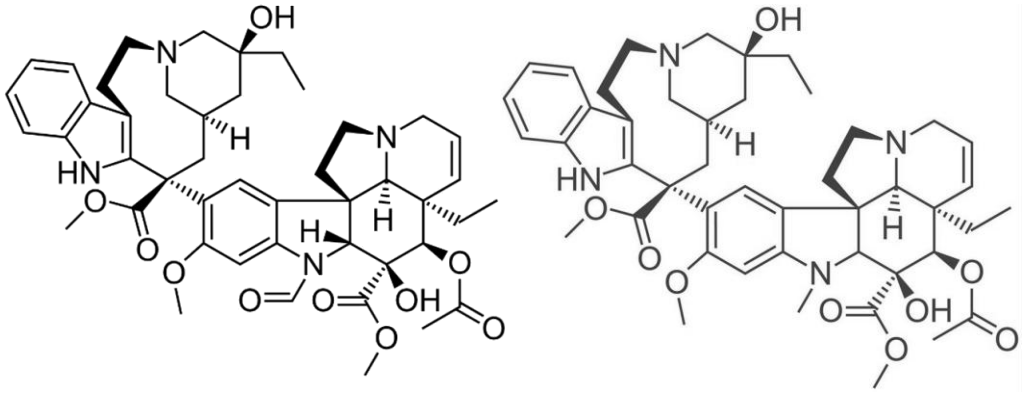

Figure 1.3: Chemical structure of Vincristine and Vinblastine

1.1.1.4 Antimicrobial Activity

The antioxidant potential in Di(1*H*-indol-3-yl)sulfane derivative was assessed (**Figure 1.4**). It showed notable antioxidant properties in various assay, including ferric reducing ability of plasma (FRAP), DPPH, and ABTS assays, all at micromolar concentrations (Kumar and Ritika, 2020).

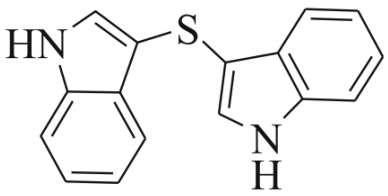

Figure 1.4: Chemical structure of Di(1*H*-indol-3-yl)sulfane

1.2 Hydrazide

A hydrazide (**Figure 1.5**) refers to a compound that contains the functional group -C(=O)-NH-NH_2, known as the hydrazide group, and is widely used in chemical reactions. This functional group enables the formation of stable covalent bonds with aldehyde and ketone groups, making hydrazides valuable for modifying and labelling biomolecules such as proteins and nucleotides (Hermanson, 2013). Hydrazides are typically synthesized by reacting hydrazine (or substituted hydrazines) with acyl derivatives such as esters. During this process, the acyl group is replaced by the hydrazide group through a nucleophilic attack by hydrazine, resulting in the formation of the hydrazide (Abdel-Aziz *et al*., 2013).

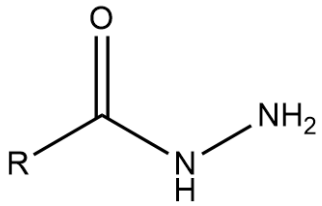

Figure 1.5: General Chemical structure of Hydrazide

1.2.1 Application of Hydrazide

Hydrazide derivatives are found in numerous bioactive molecules and display diverse biological functions, including insecticidal, herbicidal, antifungal, antitumor, and antiviral (Chang *et al*., 2023). In addition, hydrazide compounds (R-NH-NH_2) are potent, selective reagents commonly used to label carbohydrates, glycoconjugates (such as glycoproteins and glycolipids), and

reducing sugars. For example, biocytin hydrazide (BCHZ), a water-soluble, long-chain hydrazide containing biotin, was synthesized and used for the selective, non-radioactive detection of glycoconjugates (Bayer *et al*., 1988).

1.2.1.1 Anti-Inflammatory Activity

Hydrazides have shown significant anti-inflammatory, as evidenced by numerous studies. According to Cloutier *et al*. (2025), the p-Aminobenzoic acid (PABA), which shows a mild anti-inflammatory activity. Research highlighted the therapeutic value of PABA and its analogs, DAB-1, a synthetic PABA derivative incorporating both a hydrazinamide and maleimide moiety (**Figure 1.6**). DAB-1 demonstrated strong anti-inflammatory activity against multiple cell lines with relatively low toxicity. *In vivo* studies showed that DAB-1 inhibits the TNFα/NF-κB and iNOS/NO pathways to exert its anti-inflammatory effects.

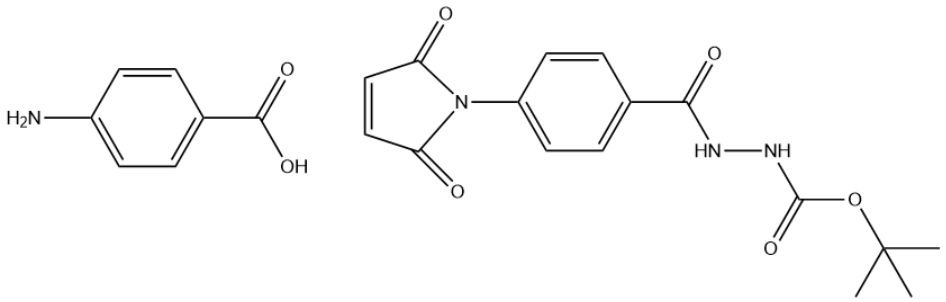

Figure 1.6: Chemical structure of PABA and DAB-1

1.2.1.2 Antibacterial Activity

Isoniazid (**Figure 1.7**) is also known as isonicotinic acid hydrazide (INH). It belongs to the class of isonicotinic acid derivatives and is primarily used as an antimicrobial agent to treat the tuberculosis. Chemically, isoniazid shares a structural similarity with nicotinic acid (vitamin B_3), nicotinamide-adenosine dinucleotide (NAD), and pyridoxine (vitamin B_6) (Cloutier *et al*., 2025). According to Kanabalan *et al*. (2021), the bactericidal activity of INH is selective for mycobacteria and the Mycobacterium Tuberculosis Complex (MTBC), which includes *Mycobacterium tuberculosis*, *Mycobacterium africanum*, *Mycobacterium bovis* and others. Its high bactericidal activity, low cost, excellent bioavailability, and effective intracellular penetration make INH a highly preferred antibacterial agent.

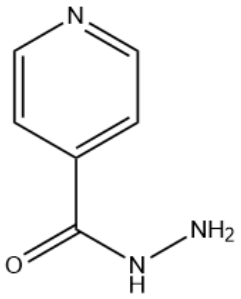

Figure 1.7: Chemical structure of Isonicotinic Acid Hydrazide

1.2.1.3 Antifungal Activity

Hydrazide compounds with heterocyclic carbonyl substituents and benzene/benzyl hydrazine side chains shows antifungal and anticancer activities. N'-phenylhydrazide based compound (**Figure 1.8**) showed strong antifungal activity against various phytopathogenic fungi, inhibiting the growth of Gibberella zeae, *Fusarium oxysporum*, *Colletotrichum higginsianum*, and *Sclerotium rolfsii* at 25 μg/mL, with inhibition rates of 98%, 91%, 100%, and 99%, respectively (Agili, 2024).

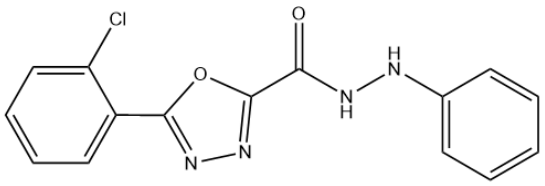

Figure 1.8: Chemical structure of *N*'-phenylhydrazide derivative

1.3 Hydrazone

N-acylhydrazones (**Figure 1.9**) are a subclass of hydrazones and are defined by the bonding of an acyl group to the hydrazone structure. It can be formed by an acid-catalyzed condensation between hydrazines (R_1-NH-NH_2) and activated carbonyl compounds, typically in methanol or ethanol solvents (Lawrence *et al*., 2019; Zhang *et al*., 2017). The *N*-acylhydrazone is a compound having the general formula of Ar-(C=O)-NH-N=CH-R, and it consists of both amide (C=O-

NH) and imine (C=N) functional groups. Besides, the moiety of –C(=O)–NH–N=CH– within the *N*-acylhydrazone possesses several reactive sites, particularly on the electrophilic carbon atom, a nucleophilic nitrogen in the imine group, and an amino nitrogen with acidic characteristics. As a result, it displays both nucleophilic and electrophilic reactivity (Shah *et al*., 2022). The amino nitrogen is typically where nucleophilic attack occurs, while the oxygen atom is responsible for electrophilic attack. Additionally, acylhydrazones can undergo keto-enol tautomerism. Besides, as the imine bond located near the nitrogen from the amide group shows acidic properties, allowing it to release a hydrogen atom from the azomethine carbon. *N*-acylhydrazones capable of forming intermolecular hydrogen bonds, like those between the hydrogen atom on the amide group's nitrogen and the oxygen atom, or between the hydrogen or nitrgen on the imine of another molecule (Socea *et al*., 2022).

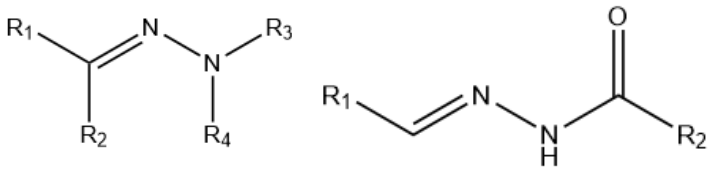

Figure 1.9: General Chemical structure of Hydrazones and *N*-acylhydrazone

1.3.1 Application of *N*-acylhydrazone

N-acylhydrazones (NAH) are attracting increasing in attention due to their broad pharmacological activities, which are attributed to the pharmacophore (–CH=N–NH–C(=O)–). Recent developments have led to bioactive NAH compounds

targeting multiple molecular sites, showing great therapeutic potential (Lim *et al.*, 2025). These compounds show pharmacological activity, such as antioxidant, analgesic, anti-inflammatory, antimicrobial, antibacterial and others (Biliz *et al*., 2023).

1.3.1.1 Anti-Inflammatory

Compound of (*E*)-*N*-(4-nitrobenzylidene)-5,6,7,8-tetrahydronaphthalene-2-carbohydrazide, known as LASSBio-1764 (**Figure 1.10**), was found to reduce leukocyte migration, TNF-α levels, and production of NO, while also inhibiting the expression of the NF-kB enzyme. Remarkably, these *N*-acylhydrazone compounds, when taken orally, did not cause any signs of myelotoxicity (Cordeiro *et al*., 2016).

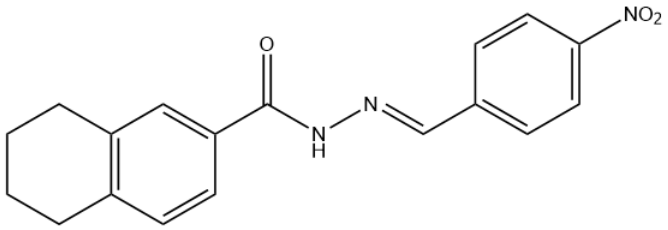

Figure 1.10: Chemical structure of LASSBio-1764

1.3.1.2 Antibacterial Activity

NAH compounds such as nitrofurazone, a broad-spectrum antibacterial agent for topical use in treating for skin infections. Nitrofurantoin and nitrofuroxazide are

oral antibacterial agents used to treat gastrointestinal infections (**Figure 1.11**). These compounds demonstrate the wide therapeutic uses of nitrofurans in combating bacterial infections (Vlad *et al*., 2024).

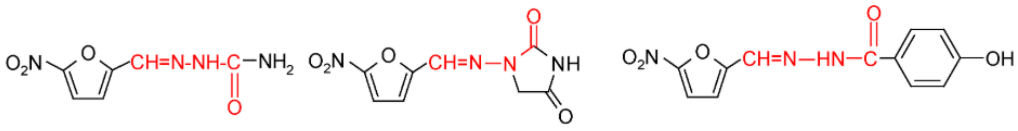

Figure 1.11: Chemical structure of Nitrofurazone, Nitrofurantoin, and Nifuroxazide

1.3.1.3 Analgesic and Cytotoxic Activity

The preliminary assessment of 1,3-thiazolidin-4-one derivatives, Compound 6 (**Figure 1.12**), showed that it is safe and non-toxic to the mice's central nervous system. It showed significant analgesic activity, probably because of the inhibition of prostaglandin production regulated by COX-2. Moreover, this compound exhibited the strongest selective cytotoxic activity against renal adenocarcinoma cells (769-P), while the growth of normal cells (H9c2, GMK) was either unchanged or only minimally reduced (Popiołek *et al*., 2018).

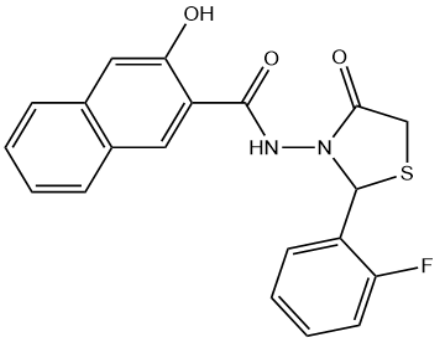

Figure 1.12: Structure of *N*-[2-(2-fluorophenyl)-4-oxo-1,3-thiazolidin-3-yl]-3-hydroxynaphthalene-2-carboxamide, Compound 6

1.3.2 Isomerism of *N*-acylhdyrazone

N-acylhydrazones can exhibit both geometrical and conformational isomerism. The presence of the imine group (–N=CH–) leads to geometric (*E*/Z) isomerism, which forms from the restricted rotation around the imine double bond (C=N). Meanwhile, the *syn*/*anti* conformational isomerism results from the rotation around the C-N single bond of the amide linkage, also known as the amide bond (C(=O)–NH). As a result, they exist as a mixture of *E* and *Z* isomers, with the *E* isomer generally being more stable and thereby more predominant compared to the *Z* isomer. Theoretically, *N*-acylhydrazones have four distinct isomers: two geometric isomers (*E*/*Z*) resulting from the C=N double bond, and two conformational isomers (*syn*/*anti*) arising from the C–N bond (Antoniolli *et al*., 2026; Socea *et al*., 2022). The *syn* conformer is more abundant than the *anti* conformer among the *E* isomers, owing to its higher stability (Kumar *et al*., 2017). The structures of these isomers are illustrated in **Figure 1.13**.

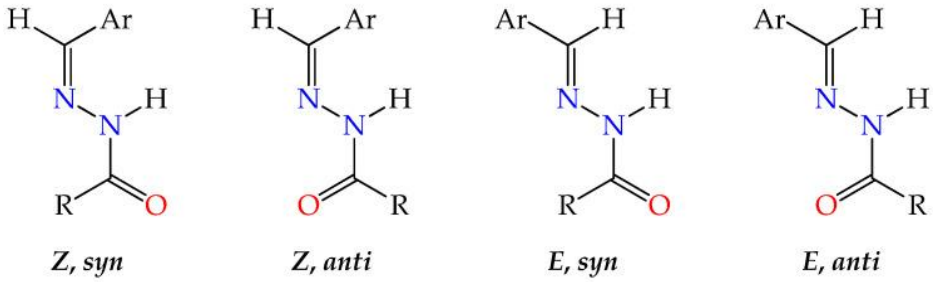

Figure 1.13: Isomers of *N*-acylhydrazone derivatives

1.4 Objectives of Research

1. To synthesize a carboxylic acid hydrazide along with a series of *N*-acylhydrazones bearing an indole ring.
2. To characterize the structure of the synthesized carboxylic acid hydrazide and *N*-acylhydrazones using various spectroscopic techniques such as FT-IR, 1D-NMR (^{1}H NMR, ^{13}C NMR and DEPT), and 2D NMR (HMQC and HMBC), and melting point analysis.
3. To evaluate the relative configuration of the imine double bond and amide group in *N*-acylhydrazones through NOE experiments.
4. To investigate the rotational barriers around the NH-C(=O) bond in *N*-acylhydrazones using Dynamic NMR experiments.

CHAPTER 2

LITERATURE REVIEW

2.1 Synthesis of Indole

Indoles are crucial in natural products and drugs, and they play an important role in cell biology. Their derivatives are increasingly recognized for their biological activity in treating cancer, infections, and various disorders (Heravi *et al*., 2021). There are several methods for synthesizing indole, which include Bartoli, Bischler, Fischer, Hemetsberger, Larock, Leimgruber-Batcho, Madelung, Nenitzescu, Reissert, and Sundberg indole synthesis (Taber and Tirunahari, 2011). The Fischer indole synthesis (**Scheme 2.1**), is one of the earliest and most versatile methods for preparing substituted indoles. It involves converting enolizable *N*-arylhydrazones into indoles and remains a widely employed approach due to its efficiency and adaptability (Çelebi-Ölçüm *et al*., 2011; Shuwirda *et al*., 2023). In this method, a phenylhydrazone is synthesized by condensing an enolizable carbonyl compound (arylhydrazone or ketone or aldehyde) with substituted phenylhydrazine, which then isomerizes to form the corresponding enamine (or 'ene-hydrazine'). After protonation, a [3,3]-

sigmatropic rearrangement occurs, forming an imine. This imine subsequently reacts to form a cyclic aminoacetal (or aminal), when heated under acidic conditions, undergoes elimination of ammonia (NH_3), and transforms into an aromatic indole. Fischer's synthesis mechanism, as proposed by Robinson (1963), consists of three key steps: (a) tautomerization of hydrazone to enehydrazine, (b) formation of C-C bond, and (c) cyclization with the elimination of ammonia, ultimately yielding indole (Sajjadifar *et al*., 2010). The mechanism is shown in the **Figure 2.1** (Inman and Moody, 2013).

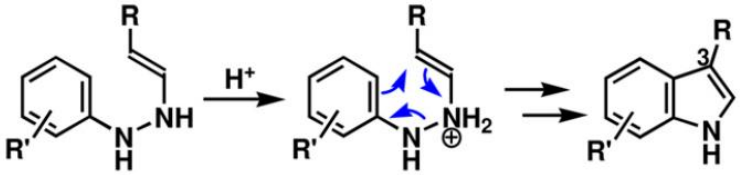

Scheme 2.1: Fischer Indole reaction

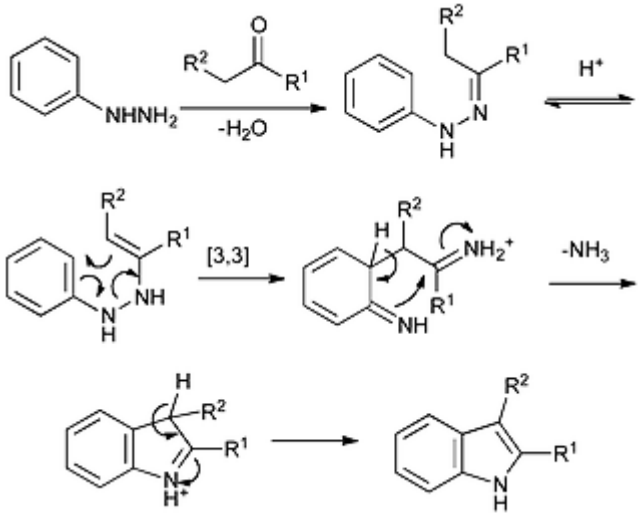

Figure 2.1: Mechanism of Fishcer Indole Synthesis

According to Li *et al*. (2019), the substituted indole compounds were synthesized via a conventional Fischer indole synthesis, using the

phenylhydrazine hydrochloride and ethyl levulinate. To synthesis the indole ester, 40 mmol of 4-substituted phenylhydrazine hydrochloride and 48 mmol of ethyl levulinate (carbonyl substrate) are carried out in the presence of 44 mmol of sodium acetate dissolved in 1M acetic acid. The mixture is then heated to 70°C and stirred for 5 to 10 minutes. The product formed is phenylhydrazone (**Scheme 2.2**). Subsequently, the synthesized phenylhydrazone is reacted with a 100 mL solution of sulfuric acid and ethanol. The reaction mixture is refluxed under heating for 3 to 4 hours and ultimately produced the indole ester (**Scheme 2.3**).

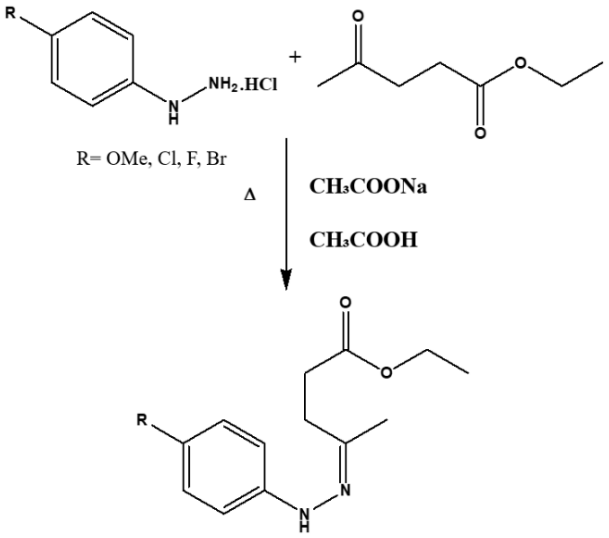

Scheme 2.2: Synthesis of Phenylhydrazone via Condensation reaction

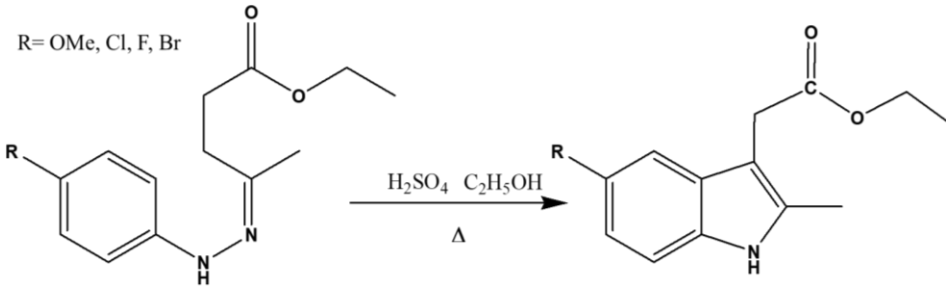

Scheme 2.3: Synthesis of Indole Ester via Cyclization reaction

A more environmental friendly approach to Fischer indole synthesis has been developed using an mechanochemical protocol, which effectively induces Fischer indolisation to produce indoles. This method uses silica gel as a solid grinding auxiliary to facilitate the reaction, as aldehydes and ketones are typically liquids. Additionally, silica gel not only success in mechanosynthesizing and also acting as a solid acid by absorbing HCl, promoting the Fischer reaction. Thus, the reaction was performed in 15 mL ZrO_2 jars with two balls (Ø = 8 mm), where *p*-tolylhydrazine hydrochloride (1a, methylated phenylhydrazine) and propiophenone (2a) were ball-milled with 300 mg of silica gel at 30 Hz for 100 minutes (Porcheddu *et al*., 2022).

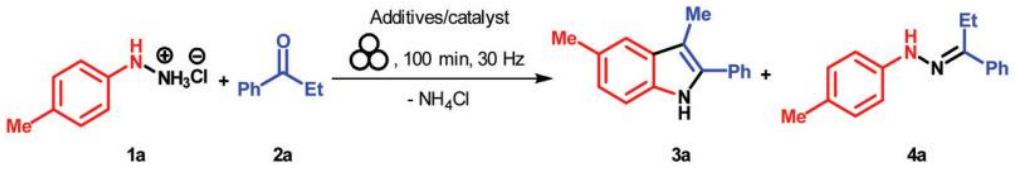

Scheme 2.4: Reaction for the Mechanochemical Fischer Indole Synthesis

2.2 Synthesis of Carboxylic Acid Hydrazide

Carboxylic acid hydrazides are important intermediates in organic synthesis they can be transformed into a variety of biologically active compounds (Teixeira *et al*., 2025). Although there are several methods can be used for the preparation, the most common use technique is the hydrazinolysis of esters using hydrazine monohydrate in ethanol, providing an efficient and straightforward route to produce hydrazides. According to Popiołek and Biernasiuk (2017), a solution of

0.01 mol of the corresponding ethyl ester of carboxylic acid was dissolved in ethanol, then refluxed with 0.011 mol of 100% hydrazine monohydrate for 2 hours. The solution was cooled to room temperature, forming a precipitate, which was then filtered, dried, and recrystallized from ethanol (**Scheme 2.5**).

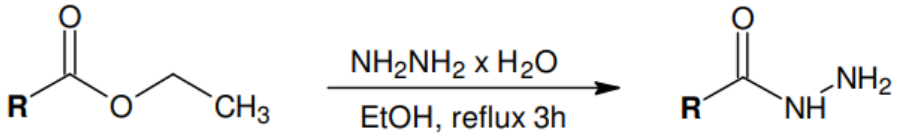

Scheme 2.5: Synthesis pathway for Nitrofurazone derivatives

According to Zhang *et al*. (2018), carboxylic acid hydrazides can be produced by the reaction between the hydrazine hydrate with the synthesized indole ester (**Chapter 2.1)** under reflux conditions in ethanol. The reaction involves 1 mmol of indole ester and 2 mmol of hydrazine hydrate in 15 mL of ethanol, refluxed for 4 hours. The final product obtained is the carboxylic acid hydrazide, with a high yield achieved (**Scheme 2.6**).

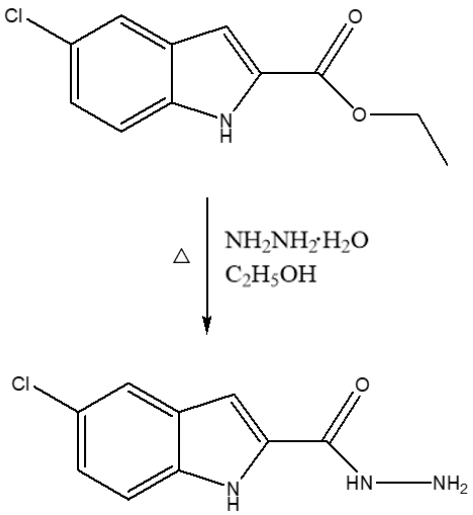

Scheme 2.6: Synthesis of Carboxylic Acid Hydrazide from Indole Ester

According to Kumar, Jakhar, and Makrandi. (2012), a simple, highly efficient, eco-friendly approach that eliminates the use of organic solvents was developed. In this method, 3.0 mmol of carboxylic acids were ground with 3.75 mmol of 80% hydrazine hydrate using a pestle and mortar for 3-5 minutes. The mixture was then allowed to digest for 10 minutes, during which it solidified. The reaction completion was monitored by thin layer chromatography. Finally, the solid was recrystallized from ethanol to obtain the hydrazides.

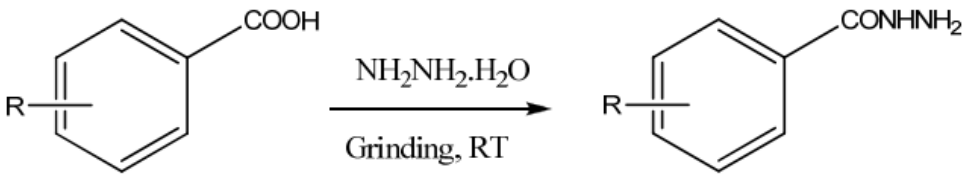

Scheme 2.7: Synthesis of Acid Hydrazides

2.3 Synthesis of *N*-acylhydrazones

N-acylhydrazone derivatives can be produced through an acid-catalyzed condensation reaction between a hydrazide precursor and various carbonyl compounds such as aromatic aldehydes or ketones (Vlad *et al*., 2024). The azomethine (NH–N=CH-) structure of these compounds contributes to their significant pharmacological activity, including antibacterial, and antioxidant activities, and their potential in drug design and medicinal chemistry.

According to Agili (2024), a mixture of 1 mmol 2-((3-Cyano-4,6-dimethyl-2-oxopyridin-1(2H)-yl)amino)-4-methylthiazole-5 carbohydrazide (3) with 1

mmol, aromatic aldehydes (4a–l) was heated in 25 mL of ethanol with a catalytic amount of glacial acetic acid for 3–4 hours, as monitored by TLC. The reaction produced hydrazide-hydrazones (5a–l), which were isolated by filtration, dried under low pressure, and recrystallized from hot ethanol (**Scheme 2.8**).

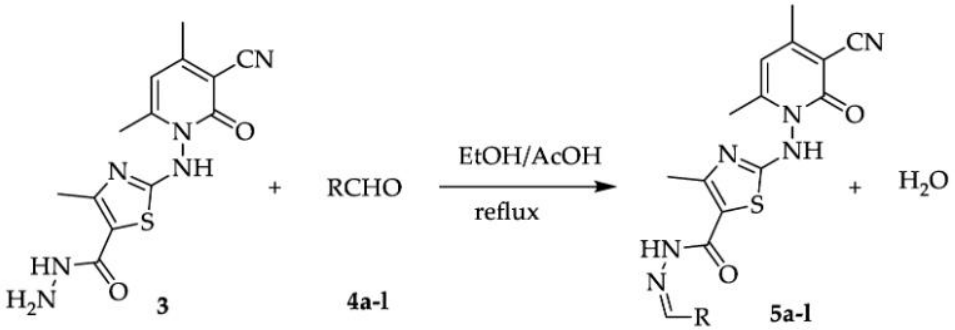

Scheme 2.8: Synthesis of Hydrazide-hydrazones derivatives

According to Mirfazli *et al*. (2014), starting materials include equimolar amounts of 1 mmol of carboxylic acid hydrazide and 1 mmol of aromatic aldehyde. The reaction was carried out using 10 mL of water as the solvent and 0.4 mL of glacial acetic acid as the catalyst. The mixture was then refluxed for 3 hours at 100°C under heating and obtained the *N*-acylhydrazone derivatives (3d–3m).

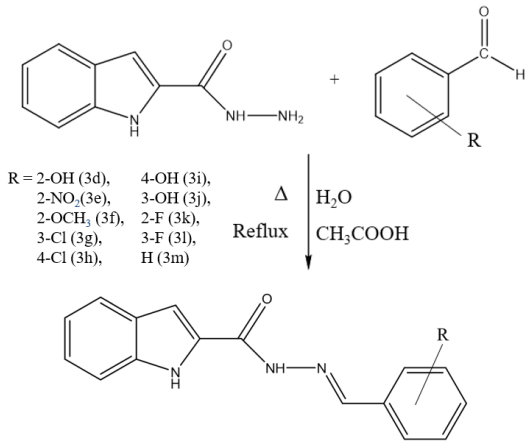

Scheme 2.9: Synthesis of *N*-acylhydrazone derivatives

According to Vlad *et al*. (2024), a green synthesis method was employed for the preparation of (*EZ*)-N′-benzylidene-2-(6-chloro-9H-carbazol-2-yl)propanohydrazide, utilizing a microwave-assisted approach. To synthesize its derivatives (1a–f), 0.001 mol of 2-(6-chloro-9H-carbazol-2-yl)propanohydrazide (4) was reacted with equimolar amount of various aromatic aldehydes in 3 mL of absolute methanol, along with four drops of glacial acetic acid added as the catalyst (**Scheme 2.10**). The reaction mixture was placed in a microwave tube, stirred for 5 minutes, and irradiated for 25 minutes at 90°C. Once the reaction was completed, the mixture was cooled to room temperature and then left overnight in the refrigerator. The product was then filtered and recrystallized using isopropanol and water in a ratio of 1:2.

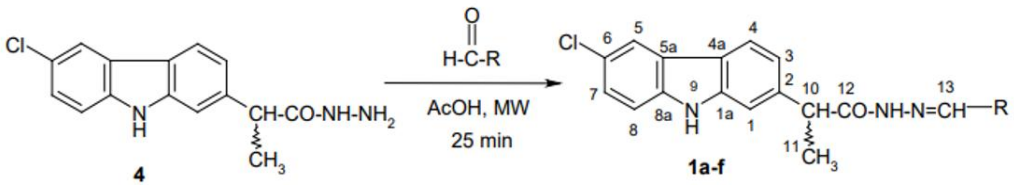

Scheme 2.10: Synthetic pathway for the novel derivative of (*EZ*)-*N*′-benzylidene-2-(6-chloro-9H-carbazol-2-yl)propanohydrazide

2.4 Conformational Study of *N*-acylhydrazones

As mentioned, *N*-acylhydrazones may exhibit a total of four isomers. Hence, NMR spectroscopy is commonly used to analyze conformational characteristics, molecular structure, spatial arrangement, and dynamics, thereby providing insights into isomer identification, interconversion, and flexibility.

2.4.1 NMR Spectra of *N*-acylhydrazones

The NMR spectra of *N*-acylhydrazones typically show duplicated signals in both ^{1}H and ^{13}C NMR. According to Lopes *et al*. (2013), during the synthesis of the analgesic LASSBio-1083 compound, the observed duplication of signals might be attributed to the presence of two possible isomers resulting from the C-N bond.

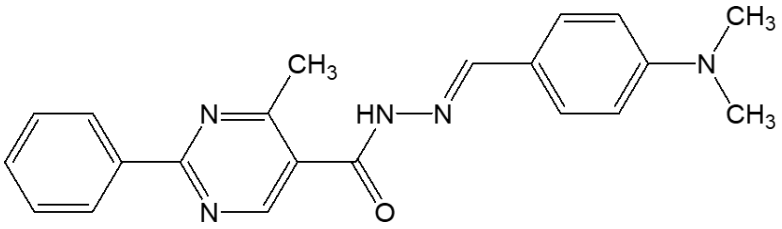

Figure 2.2: Chemical structure of compound LASSBio-1083

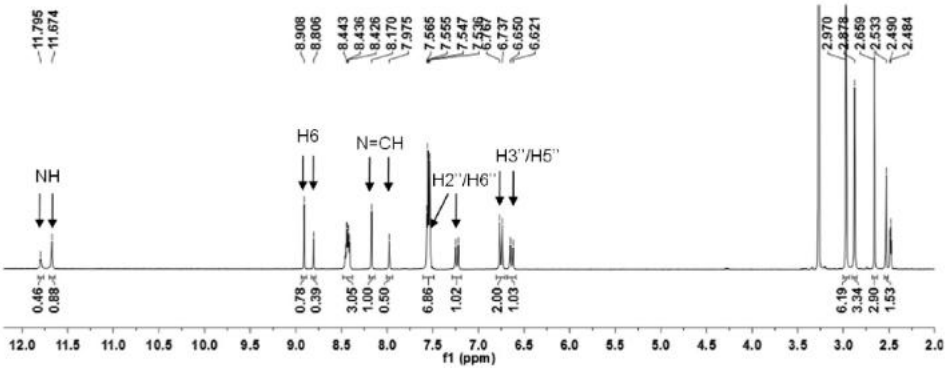

Figure 2.3: ^{1}H NMR spectrum of compound LASSBio-1083

According to Munir *et al*. (2021), two NH signals from the compound, as shown in **Figure 2.3** were detected. Thus, the integration of both NH signals from the antiperiplanar and synperiplanar conformers can be used in the identification of

both conformers. The antiperiplanar shifted further downfield than the synperiplanar.

2.4.2 Determination of the relative configuration of *N*-acylhydrazones

According to Lopes *et al.* (2013), the relative configuration of LASSBio-1083 compound can be investigated by using differential Nuclear Overhauser Effect (NOEdiff) experiments with irradiating the amide proton (NH). The findings suggest that only the *E* isomer was detected, due to the favorable spatial orientation and steric factors whereas the *Z* isomer may have a less favorable arrangement, leading to weaker or undetectable signals in the NOEdiff spectra (Munir *et al*., 2021). The spectra can be seen in **Figures 2.4** and **2.5**.

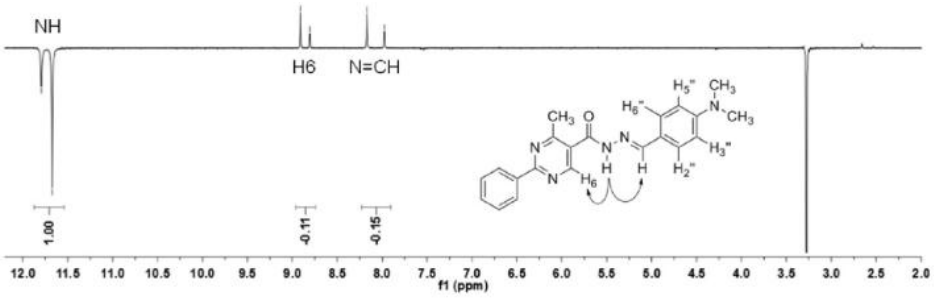

Figure 2.4: NOEdiff spectra for N<u>H</u> irradiation on compound LASSBio-1083

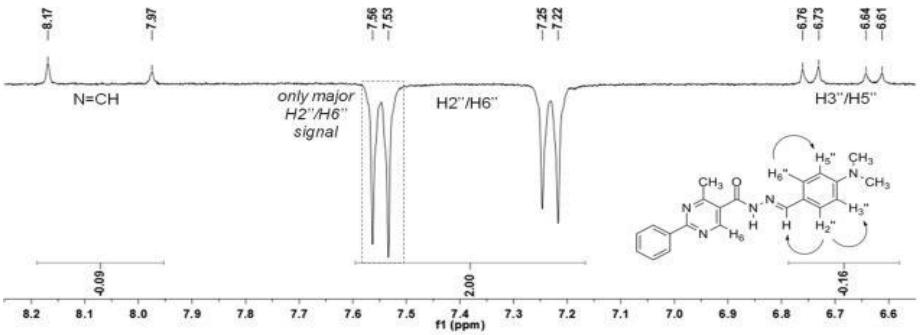

Figure 2.5: Expanded NOEdiff spectra for H2”/H6” irradiation on compound LASSBio-1083

2.4.3 Dynamic Studies of the CO-NH Rotational Barrier

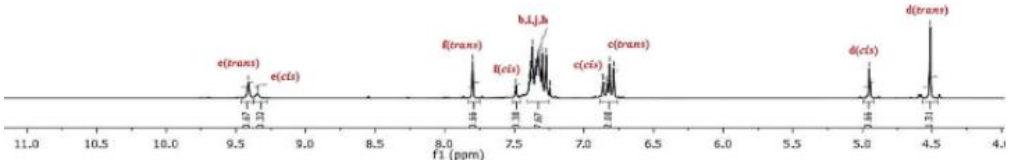

Figure 2.6: The ^{1}H NMR spectrum of *N*-acylhydrazone derivative in DMSO-d_6

The presence of the C-N bond within the amide group in the *N*-acylhydrazone leads to the formation of two conformers (Vlad *et al*., 2024). Therefore, two conformational isomers (*syn*/*anti*) of *N*-acylhydrazones exist in equilibrium, which results in their appearance in the NMR spectrum (**Figure 2.6**). The coalescence temperature measured during a dynamic NMR experiment can be used to determine the rotational barrier between these isomers (Munir *et al*., 2021). According to Hamzi, Barhoumi-Slimi and Abidi (2016), found that as the temperature increases, the energy required to overcome the rotational barrier is reached, allowing rapid interconversion between the conformers. In the coalescence temperature method, the compound is gradually heated until the *syn* and *anti* signals coalescence. The coalescence temperature (T_c) is reached when these signals combine into a broad singlet peak. Thus, the coalescence temperature (T_c) can be used to calculate the rate constant (k_c) by using the equation $k_c = (\pi \times \Delta\nu)/\sqrt{2}$, where the peak separation ($\Delta\nu$) obtained from spectra recorded at temperatures below the coalescence. Thus, the Gibbs free energy of activation ($\Delta G^{\neq}$) can be determined by using the Eyring equation: $\Delta G^{\neq} = 19.14T_c (10.32 + \log \frac{T_c}{k_c}) \times 10^{-3}$, with units in kJ/mol. The synthesized *N*-acylhydrazones

and its ^{1}H NMR spectrum at various temperature are shown in **Figures 2.7** and **2.8**.

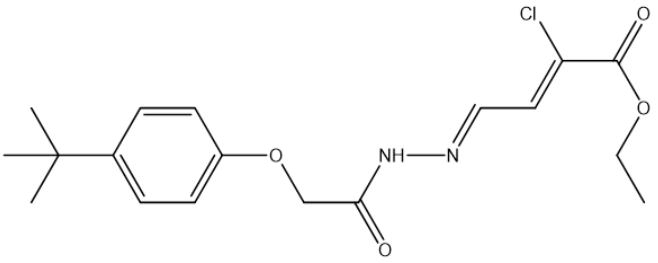

Figure 2.7: Chemical structure of the synthesized *N*-acylhydrazone

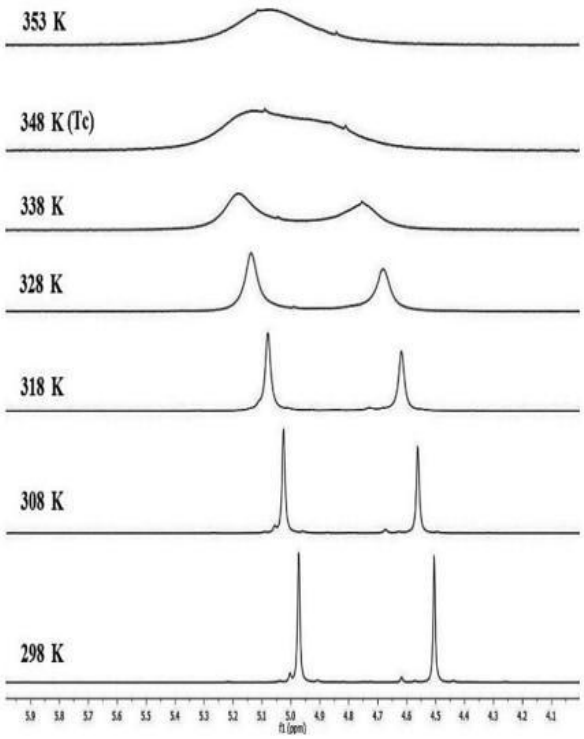

Figure 2.8: ^{1}H NMR spectra of the -OCH_2 signals of the Synthesized *N*-acylhydrazone in DMSO-d_6 at variable temperatures

CHAPTER 3

MATERIALS AND METHODOLOGY

3.1 Chemicals Used

The chemicals involved for the synthesis of carboxylic acid hydrazide, the synthesis and recrystallization of *N*-acylhydrazones, TLC analysis, determination of antioxidant activity, IR and NMR characterization are summarized in **Tables 3.1** to **3.8**.

Table 3.1: Chemicals used for the synthesis of Indole Ester

Chemicals Name Molecular Formula	**Molecular Weight $gmol^{-1}$**	**Manufacturer, Country**	**State**	**Purity**
Absolute Ethanol C_2H_5OH	46.07	Fischer Scientific, UK	Liquid	99.90%
Concentrated Hydrochloric Acid HCl	36.46	Fischer Scientific, UK	Liquid	-
Ethyl Acetate	88.11	RCI Labscan,	Liquid	99.50%

$CH_3COOC_2H_5$		Thailand		
Anhydrous Sodium Sulphate Na_2SO_4	142.04	Merck, Germany	Solid	≥99.0%

Table 3.2: Chemicals used for the synthesis of Carboxylic Acid Hydrazide

Chemicals Name Molecular Formula	**Molecular Weight $gmol^{-1}$**	**Manufacturer, Country**	**State**	**Purity**
Hydrazine hydrate $NH_2NH_2{\cdot}H_2O$	50.06	Synerlab, France	Liquid	80.00%
Ethyl Acetate $CH_3COOC_2H_5$	88.11	RCI Labscan, Thailand	Liquid	99.50%
Absolute Ethanol C_2H_5OH	46.07	Fischer Scientific, UK	Liquid	99.90%
Anhydrous Sodium Sulphate Na_2SO_4	142.04	Merck, Germany	Solid	≥99.0%

Table 3.3: Chemicals used for the synthesis of *N*-acylhydrazone

Chemicals Name Molecular Formula	**Molecular Weight**	**Manufacturer, Country**	**State**	**Purity**

	$gmol^{-1}$			
2-Hydroxybenzaldehyde $C_7H_6O_2$	122.12	Merck, Germany	Liquid	≥95.0%
3-Hydroxybenzaldehyde $C_7H_6O_2$	122.12	ChemScence, China	Solid	99.84%
4-Hydroxybenzaldehyde $C_7H_6O_2$	122.12	Merck, Germany	Solid	≥98.0%
2-Chlorobenzaldehyde C_7H_5ClO	140.57	Merck, Germany	Liquid	≥95.0%
4-Chlorobenzaldehyde C_7H_5ClO	140.57	Merck, Germany	Solid	98.00%
2,4-Dichlorobenzaldehyde $C_7H_4Cl_2O$	175.01	Merck, Germany	Solid	98.00%
4-Methylbenzaldehdye C_8H_8O	120.15	Merck, Germany	Liquid	≥97.0%
Benzaldehyde C_7H_6O	106.12	Gene Chemicals, China	Liquid	≥99.0%
4-Methoxybenzaldehyde	136.15	Acros Organics,	Liquid	≥99.0%

$C_8H_8O_2$		USA		
4-Nitrobenzaldehyde $C_7H_5NO_3$	151.12	Merck, Germany	Solid	99.00%
L-(+)-Tartaric Acid $(CHOH{\cdot}COOH)_2$	150.09	Fischer Scientific, UK	Solid	99.80%
Absolute Ethanol C_2H_5OH	46.07	Fischer Scientific, UK	Liquid	99.90%

Table 3.4: Chemicals used for the Recrystallization

Chemicals Name Molecular Formula	**Molecular Weight $gmol^{-1}$**	**Manufacturer, Country**	**State**	**Purity**
95% Ethanol C_2H_5OH	46.07	Chemical Industries (Malaya), Malaysia	Liquid	96.00%

Table 3.5: Chemicals used in Thin Layer Chromatography Analysis

Chemicals Name Molecular Formula	**Molecular Weight $gmol^{-1}$**	**Manufacturer, Country**	**State**	**Purity**
TLC Plate	-	Merck, Germany	-	-

95% Ethanol C_2H_5OH	46.07	Chemical Industries (Malaya), Malaysia	Liquid	96.00%
Chloroform $CHCl_3$	119.38	Merck, Germany	Liquid	99.00-99.40 %
Ethyl Acetate $CH_3COOC_2H_5$	88.11	RCI Labscan, Thailand	Liquid	99.50%
n-Hexane $CH_3(CH_2)_4CH_3$	86.18	RCI Labscan, Thailand	Liquid	99.00%

Table 3.6: Chemicals used in IR characterization of *N*-acylhydrazones

Chemicals Name Molecular Formula	**Molecular Weight $gmol^{-1}$**	**Manufacturer, Country**	**State**	**Purity**
Potassium Bromide KBr	119.00	Sigma Aldrich, China	Solid	≥99.0%

Table 3.7: Chemicals used in NMR characterization of *N*-acylhydrazones

Chemicals Name Molecular Formula	**Molecular Weight $gmol^{-1}$**	**Manufacturer, Country**	**State**	**Purity**

Dimethyl Sulfoxide-d_6 (DMSO-d_6) $(CD_3)_2SO$	78.13	Fischer Scientific, UK	Liquid	≥99.0%

3.2 Instruments Used

The instruments involved are listed in **Table 3.8**.

Table 3.8: Instruments Used

Instrument	Manufacturer	Model
Nuclear Magnetic Resonance Spectrometer	Jeol	JNM-ECX-400
Fourier Transform Infrared Spectrometer	Perkin Elmer	Spectrum RX1
Melting Point Apparatus	Stuart	SMP 10
Rotary Evaporator	BUCHI	R-200, Heating Bath B-491
Ultrasonic Bath	Bransonic	5510E-DTH

3.3 Experiment Procedure

The synthesis of *N*-acylhydrazones was carried out, which can be divided into two main steps, as outlined below.

3.3.1 Synthesis of Indole Ester

For the preparation of, a mixture of 50 mmol of and 65 mmol of were added to a 250 mL round-bottom flask, followed by the addition of 70 mL acid to dissolve the reactants. Then, a small amount of boiling chips and a magnetic stir bar were then introduced into the flask. The reaction mixture was then heated in an oil bath at 80 °C for 6 hours using a magnetic stirrer hotplate, with the temperature monitored by a thermometer. The progress of the reaction was monitored using thin-layer chromatography (TLC) to determine when it had reached completion.

After completion, the reaction mixture was poured into a beaker with crushed ice and stirred. The formed was extracted three times with approximately 40 mL portions of ethyl acetate. The combined organic layers were dried using anhydrous sodium sulfate to eliminate residual moisture. Finally, the solvent ethyl acetate was removed under reduced pressure using a rotary evaporator, yielding the, which was then used in the subsequent synthesis step.

For the synthesis of the indole ester, the first step was again placed into a 250 mL round-bottom flask. Then, 25 mL of absolute ethanol was added, followed by the addition of 2 mL of acid. The reaction mixture was then heated under reflux in an oil bath at 80 °C for 6 hours using a magnetic stirrer hotplate, with

the temperature continuously monitored using a thermometer. Reaction progress was monitored by thin-layer chromatography (TLC) to determine when the reaction was complete. After completion, the reaction mixture was cooled to room temperature and poured into a beaker containing crushed ice, then stirred. The indole ester was extracted three times with 40 mL portions of ethyl acetate. The organic layers were combined and dried using anhydrous sodium sulfate. Finally, the solvent ethyl acetate was evaporated under reduced pressure with a rotary evaporator to yield the indole ester.

3.3.2 Synthesis of Carboxylic Acid Hydrazide

To synthesize carboxylic acid hydrazide, the indole ester was placed into a 250 mL round-bottom flask. Next, 70 mL of hydrazine hydrate and 25 mL of absolute ethanol were added, along with boiling chips and a magnetic stir bar. The reaction mixture was then heated under reflux in an oil bath at 80 °C for 6 hours using a magnetic stirrer hotplate, with the temperature continuously monitored using a thermometer. Reaction progress was monitored by thin-layer chromatography (TLC) to determine when it had reached completion. Once finished, the mixture was cooled to room temperature and poured into a beaker with crushed ice and stirred. The resulting carboxylic acid hydrazide was

extracted three times with 40 mL portions of ethyl acetate. The organic layers were dried using anhydrous sodium sulfate. Finally, the solvent ethyl acetate was evaporated under reduced pressure using a rotary evaporator to produce the crude carboxylic acid hydrazide. To purify the crude carboxylic acid hydrazide, it was recrystallized by dissolving in hot 95% ethanol and filtering through cotton wool. The filtrate was concentrated by heating. Then, it was allowed to cool and left at room temperature for solvent evaporation. The resulting solid was washed with cold 95% ethanol and finally dried in an oven at 80 °C.

3.3.3 Synthesis of *N*-acylhydrazones

To synthesize the *N*-acylhydrazones, 2 mmol of the prepared carboxylic acid hydrazide was refluxed with 2 mmol of the respective benzaldehydes listed in **Table 3.10**.

Table 3.10: Various benzaldehydes used in synthesis of *N*-acylhydrazones

Benzaldehyde	**Molecular Weight ($gmol^{-1}$)**	**2 mmol**	
		Mass (g)	**Volume (mL)**
2-Hydroxybenzaldehyde $C_7H_6O_2$	122.12	-	0.211

3-Hydroxybenzaldehyde $C_7H_6O_2$	122.12	0.2442	-
4-Hydroxybenzaldehyde $C_7H_6O_2$	122.12	0.2442	-
2-Chlorobenzaldehyde C_7H_5ClO	140.57	-	0.225
4-Chlorobenzaldehyde C_7H_5ClO	140.57	0.2811	-
2,4-Dichlorobenzaldehyde $C_7H_4Cl_2O$	175.01	0.3500	-
4-Methylbenzaldehdye C_8H_8O	120.15	-	0.236
Benzaldehyde C_7H_6O	106.12	-	0.204
4-Methoxybenzaldehyde $C_8H_8O_2$	136.15	-	0.243
4-Nitrobenzaldehyde $C_7H_5NO_3$	151.12	0.3022	-

Equimolar amounts (2 mmol) of carboxylic acid hydrazide and of benzaldehyde with different substituents were added to a 50 mL round-bottom flask, along with the addition of catalyst. The reaction mixture was dissolved in about 15 mL of absolute ethanol with the aid of sonication. After adding boiling chips and a

magnetic stir bar, the mixture was then heated under reflux in an oil bath at approximately 80 °C for 8 hours using a magnetic stirrer hot plate, with the temperature continuously monitored with a thermometer. Again, reaction progress was checked by thin-layer chromatography (TLC) to confirm completion.

After reflux, the reaction mixture was allowed to cool in room temperature and then poured into crushed ice in a beaker. It was stirred and left to stand overnight to allow precipitation. The crude product was collected by vacuum filtration. During filtration, it was washed with distilled water to remove residual any unreacted starting materials. The crude solid was then purified by recrystallization using hot 95% ethanol.

3.3.4 Purification by Recrystallization

The crude product was purified by recrystallization using a minimal amount of hot 95% ethanol to dissolve the solid. The resulting solution was then subjected to hot filtration, during which insoluble impurities of the solution were removed by filtering through cotton wool in a gravity glass funnel into a clean beaker. Next, boiling chips were added to prevent overheating and bumping. The filtrate was then concentrated by heating until the volume was reduced to approximately 25 mL or until solid formation, after which it was removed from the hotplate. The solution was allowed to cooled in room temperature to allow crystallization to occur. The formed crystals were rinsed with a small amount of cold ethanol

and then dried in an oven at 80 °C. Finally, the dried product was weighed and recorded.

3.4 Characterization

The synthesized products were characterized using several analytical methods, including 1-D & 2-D NMR, FTIR spectroscopy, thin-layer chromatography (TLC), and melting point analysis.

3.4.1 Melting Point Determination

The melting points of all synthesized compounds were determined as an indication of their purity. A pure compound usually shows a sharp range of melting points, while impurities present tend to broaden it. Therefore, a narrow melting point range reflects higher purity, whereas a wider range suggests the presence of impurities.

A melting point apparatus was used to measure the melting point. A small amount of each compound was packed into a haematocrit capillary tube, gently tapped to compact it, and then placed into the apparatus. The temperature was set and gradually increased up to 300 °C, as the expected melting range of the

compounds was below ~280 °C. The temperature increased slowly, and the range of temperatures at which the solid began to melt and fully melted was recorded as the melting point range. Each measurement was repeated at least three times to ensure the accuracy and precision of the results.

3.4.2 Fourier Transform Infrared (FTIR) Spectroscopy

FTIR spectroscopy is a technique used to identify the presence of functional groups within a molecule. It works by measuring the infrared radiation absorption, where different bonds absorb at specific IR frequencies. As a result, functional groups can be identified by specific wavenumber ranges, since different chemical bonds absorb infrared radiation at different frequencies. Therefore, FTIR spectroscopy was used to provide structural information by identifying the functional groups in the synthesized compounds with reference to standard IR absorption data.

As anhydrous potassium bromide (KBr) does not absorb infrared radiation, it is commonly used as a matrix material without causing interference. However, it must be stored in an oven to avoid moisture absorption from the air, which could lead to IR interference. For sample preparation, the solid compound was mixed with KBr in a ratio of approximately 1:10 and finely ground into a fine powder using a pestle and mortar. The homogeneous mixture was then compressed into

a translucent pellet using a pellet press for analysis. The prepared pellet was placed into the FTIR spectrometer and scanned in the mid-infrared region, typically from 4000 to 400 cm^{-1}.

3.4.3 Nuclear Magnetic Resonance (NMR) Spectroscopy

Nuclear Magnetic Resonance (NMR) is a physical phenomenon where atomic nuclei exhibit magnetic behavior when exposed to a strong external magnetic field. NMR spectroscopy provides details on the number of magnetically non-equivalent atoms in a compound, particularly for nuclei such as hydrogen-1 (^{1}H) and carbon-13 (^{13}C). As a result, NMR spectroscopy is an essential tool in organic chemistry, as it offers important information about the chemical environment of specific nuclei within a molecule. The most commonly used forms are proton NMR (^{1}H NMR) and carbon-^{13} NMR (^{13}C NMR).

To differentiate carbon types such as methyl, methylene, methine, and quaternary carbons in the ^{13}C NMR spectra, DEPT (Distortionless Enhancement by Polarization Transfer) was employed. While HMQC (Heteronuclear Multiple Quantum Correlation) was then used to detect direct one-bond correlations between protons and their attached carbons, and HMBC (Heteronuclear Multiple Bond Correlation) was used to detect long-range proton–carbon couplings. The combination of these spectral data enabled the structural elucidation of the synthesized compounds.

To prepare the sample, approximately 25 mg of each product was weighed and dissolved in a small volume of DMSO-d_6 in a clean vial. The solution was then carefully transferred into an NMR tube, reaching a height of approximately 4 cm from the bottom, labelled, and submitted for analysis.

3.4.4 Thin Layer Chromatography (TLC)

Thin Layer Chromatography (TLC) was used to assess product purity and monitor reaction progress. In this technique, the solvent or solvent mixture acted as the mobile phase, while the silica gel on the TLC plate served as the stationary phase. The purity of a compound was evaluated based on the number and appearance of spots observed under ultraviolet light. For TLC analysis, a small amount of the synthesized compound was first dissolved in a clean vial using a minimal volume of ethanol, followed by chloroform, and sonicated to ensure complete dissolution. The baseline and solvent front were marked approximately 1 cm each from the bottom and top edges of the TLC plate. A concentrated enough amount of sample was then spotted onto the baseline using a capillary tube. To prevent overlapping, the spots were spaced between 1 cm and at least 0.5 cm from the edge of the plate.

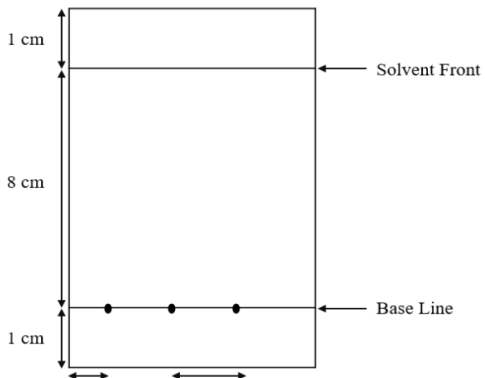

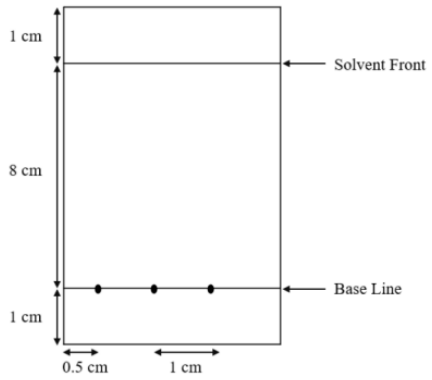

Figure 3.1: TLC Plate

The TLC plate (**Figure 3.1**) was placed in a chamber containing a mixture of hexane and ethyl acetate in a 1:1 ratio as the developing solvent. Once the solvent reached the solvent front, the plate was removed from the chamber and allowed to dry. The separated spots were visualized under a 254 nm ultraviolet lamp and marked with a 2B pencil, or alternatively, placed in an iodine chamber. The retardation factor (R_f) values of the observed spots were then calculated.

3.5 Calculation

The following formulas were applied to perform the calculations and are presented below.

- The mass of the starting material:

  Mass (g) = Number of moles (mol) × Molecular Mass (g/mol)

- The volume required of the starting material:

$$\text{Volume (mL)} = \frac{\text{Number of moles (mol)} \times \text{Molecular Mass (g/mol)}}{\text{Density (g/mL)}}$$

- Percentage yield of product synthesized:

$$\text{Percentage Yield (\%)} = \frac{\text{Experimental Yield (g)}}{\text{Theoretical Yield (g)}} \times 100\%$$

- Retardation factor (R_f)

$$\text{Retardation factor} = \frac{\text{Distance travelled by sample/analyte (cm)}}{\text{Distance travelled by mobile phase from the base line (cm)}}$$

CHAPTER 4

RESULTS AND DISCUSSION

4.1 Molecular Structure of the Synthesized Compounds

In this study, a total of eleven compounds were prepared, including one carboxylic acid hydrazide and ten *N*-acylhydrazone derivatives. Their corresponding codes, corresponding IUPAC systematic names, and molecular structures are summarized in **Table 4.1**.

Table 4.1: Codes, names, and structures of the synthesized compounds

4.2 Synthesis and Proposed Mechanism of Indole Ester

The synthesis of carboxylic acid hydrazide began with the formation of the indole ester, which was then converted into the carboxylic acid hydrazide.

The formation of the indole ester consists of two reactions, which are a condensation reaction and a cyclization reaction.

Hence, an indole ester can be synthesized via the pathway illustrated in **Scheme**

4.1, and the mechanism is shown in **Figure 4.1**.

Scheme 4.1: Synthetic route for Indole Ester

Figure 4.1: Mechanism for the Synthesis of Indole Ester

4.3 Synthesis and Proposed Mechanism of Carboxylic Acid Hydrazide

To synthesize the carboxylic acid hydrazide, the previously synthesized indole ester was reacted with hydrazine hydrate. This reaction proceeded through nucleophilic attack by the nitrogen atom of hydrazine, which has a lone pair of electrons, on the ester's carbonyl carbon. During this nucleophilic substitution, the ethoxy group bonded to the carbonyl carbon will act as the leaving group. This reaction proceeds via nucleophilic acyl substitution, in which the electrophilic carbonyl carbon of the ester is attacked by the nitrogen atom of hydrazine, possessing a lone pair of electrons, to form an intermediate. This intermediate subsequently collapses with the removal of the ethoxide ion as the leaving group. Therefore, a fast proton transfer then occurs, producing the corresponding acetohydrazide as the main product and ethanol as a by-product (Ibrahim *et al*., 2013). Overall, the carboxylic acid hydrazide can be synthesized via the multistep pathway illustrated in **Scheme 4.2**, and the mechanism given in **Figure 4.2**.

Scheme 4.2: Synthetic route of Carboxylic Acid Hydrazide

Figure 4.2: Mechanism for the synthesis of Carboxylic Acid Hydrazide

4.3.1 Discussion on Carboxylic Acid Hydrazide

The carboxylic acid hydrazide was obtained as a light brown solid at room temperature. It gave a percentage yield of 49% and exhibited a melting point in the range of °C. The retardation factor (R_f) was determined using thin-layer chromatography (TLC) with a solvent system of ethyl acetate and hexane in a 1:1 volume ratio, resulting in an R_f value of 0.05. A summary of its physical characteristics is provided in **Table 4.2**.

Table 4. 2: Physicochemical properties of carboxylic acid hydrazide

The structure of carboxylic acid hydrazide is shown in **Figure 4.3**.

Figure 4.3: Structure and numbering of carboxylic acid hydrazide

Figure 4.4: FT-IR (KBr, cm^{-1}) spectrum of carboxylic acid hydrazide

Based on the IR spectrum shown in **Figure 4.4**, the carboxylic acid hydrazide displays several characteristic absorption bands consistent with its functional groups. Medium-intensity absorptions around 3067 and 2908 cm^{-1} correspond to aromatic sp^2 C–H stretching and aliphatic sp^3 C–H stretching, respectively and consistent with literature ranges. It indicating the presence of both aromatic ring and saturated carbon in the compound. A strong and sharp peak at 1677 cm^{-1} was assigned to the carbonyl (C=O) stretching vibration of the hydrazide moiety, while the adjacent strong band at 1636 cm^{-1} was associated with aromatic C=C stretching. At lower wavenumbers, the band at 1234 cm^{-1} was assigned to C–N stretching vibration. The IR spectral data, along with the observed functional group assignments and their corresponding wavenumbers, were summarised in **Table 4.3**.

Table 4.3: Summary of FTIR spectral data of carboxylic acid hydrazide

The ^1H NMR spectrum of the carboxylic acid hydrazide (**Figure 4.5)** showed two signals in the deshielded region. A singlet at δ is assigned to the proton (H-1), which appears at the most downfield. In aromatic systems, the π-electron cloud circulates under the influence of an external magnetic field, generating an induced magnetic field that deshields nearby protons, causing them to appear at higher chemical shift values (downfield) due to the strong aromatic ring current effect (Abraham *et al*., 2000; Bradley *et al*., 2023). Another singlet appeared at δ belongs to the hydrazide..

Multiple signals were observed in the region δ 6 ppm, which were attributed to the aromatic protons of the phenyl rings (Salih *et al*., 2020).

The ^{13}C NMR spectrum (**Figure 4.6**) displays distinct signals, consistent with non-equivalent carbon atoms. The carbonyl carbon (C9) appears at δ, consistent with a highly deshielded sp^2-hybridised carbonyl carbon bonded to oxygen. This downfield shift is attributed to the strong electron-withdrawing effect of the oxygen atom and the diamagnetic anisotropy nature of the C=O double bond, which together reduce electron density at the carbon nucleus, resulting in pronounced deshielding and a signal appearing at the far downfield region (Farmer, Soderberg and Schaller, 2016; Martin *et al*., 2003).

The carbon types were further differentiated by DEPT-135 NMR spectroscopy, which identified one methyl, one methylene, and three methine carbons (Atta-ur-Rahman *et al*., 2016). Methyl and methine carbons appear as positive signals, while methylene carbons appear in the negative region (Santos & Silva, 2014). The methyl carbon is more shielded compared to the methine carbons. Therefore, by comparison with the DEPT-135 spectrum and the ^{13}C NMR spectrum, a total of six quaternary carbons were identified (**Figure 4.7**). The ^{1}H and ^{13}C NMR spectral data are summarised in **Table 4.4**.

Furthermore, heteronuclear multiple quantum coherence (HMQC) is a 2D-NMR technique that provides direct single-bond correlations between protons and their directly attached carbon atoms (Claridge, 2016). From the HMQC spectrum (**Figure 4.8**), a total of five correlations are observed at δ_H 7/δ_C, δ_H 7/δ_C, δ_H 6/δ_C ,

$\delta H / \delta_C$, and δ_H / δ_C representing the correlation.

Moreover, heteronuclear multiple quantum coherence (HMQC) is a 2D-NMR technique that provides direct single-bond correlations between protons and their directly attached carbon atoms (Claridge, 2016). In contrast, heteronuclear multiple bond correlation (HMBC) reveals long-range (around two to four-bond) $^{13}C–^{1}H$ correlations and provides connectivity information between neighbouring atoms (Agarwal *et al*., 2018). Unlike HMQC, HMBC does not show direct one-bond correlations. In the HMBC spectrum (**Figure 4.9**), corresponding to three-bond and two-bond couplings, respectively. No correlation is observed with the directly bonded methyl carbon, consistent with the expected behaviour of HMBC experiments, which usually do not display one-bond correlations.

Therefore, by integrating the results from ^{1}H, ^{13}C, DEPT-135, HMQC, and HMBC analyses, the characterization of the structure of carboxylic acid hydrazide can be determined through the reliable assignment of both proton and carbon signals.

Table 4.4: Summary of ^{1}H and ^{13}C NMR spectral data of carboxylic acid hydrazide

Figure 4.5: ^{1}H NMR (400 MHz, DMSO-d_6) spectrum of carboxylic acid hydrazide

Figure 4.6: ^{13}C NMR (100 MHz, DMSO-d_6) spectrum of carboxylic acid hydrazide

Figure 4.7: DEPT spectrum of carboxylic acid hydrazide

Figure 4.8: HMQC spectrum of carboxylic acid hydrazide

Figure 4.9: HMBC NMR spectrum of carboxylic acid hydrazide

4.4 Synthesis and Proposed Mechanism of *N*-acylhydrazones SB 1-SB 10

The *N*-acylhydrazone derivatives **(SB 1–SB 10)** bearing an indole moiety are synthesised through the condensation reaction between the synthesized carboxylic acid hydrazide and various substituted benzaldehydes. In this reaction, two reactants are involved, which are the carboxylic acid hydrazide precursor and the corresponding benzaldehyde derivatives (Pai and Bhat, 2026).

The mechanism (**Figure 4.10**) starts with the terminal $–NH_2$ group of the carboxylic acid hydrazide acting as a nucleophile, responsible for attacking the electrophilic carbonyl carbon of the benzaldehyde, leading to the formation of an alkoxide, which serves as an intermediate. This intermediate subsequently undergoes proton transfer from the nitrogen to oxygen, thereby converting it into a carbinolamine species. Subsequently, it undergoes dehydration, leading to the formation of the imine (C=N) bond (Badawy *et al*., 2025).

Finally, deprotonation of the nitrogen atom produced the desired *N*-acylhydrazone product with establishing the characteristic –C(=O)–NH–N=C– *N*-acylhydrazone linkage. Throughout the process, acid functions as a catalyst and is regenerated at the end of the reaction. Its effectiveness, together with its environmentally benign nature as it is naturally derived from fruits such as grapes, makes acid a suitable catalyst for the condensation of aromatic aldehydes with amines in alcoholic solvents (Ukaji & Soeta, 2012). In addition, its good

solubility in both water and ethanol, where ethanol is used as the solvent in the synthesis of the desired *N*-acylhydrazone further enhances its compatibility in the reaction system (Li *et al*., 2023). As a result, the reaction can proceed under mild conditions, producing good yields within a shorter reaction time (Aboonajmi *et al*., 2015). The *N*-acylhydrazone can be synthesized via the synthethic route as outlined in **Scheme 4.3**.

Scheme 4.3: Synthetic route of *N*-acylhydrazones

Figure 4.10: Mechanism for the synthesis of *N*-acylhydrazones

4.4.1 Physicochemical Properties of Synthesized *N*-acylhydrazone

Figure 4.11: General structure and numbering of *N*-acylhydrazones

A series of ten *N*-acylhydrazone derivatives (**SB 1–SB 10**) were successfully synthesized through the condensation reaction described earlier, and their general structure was illustrated in **Figure 4.11**. The substituents (R) attached to the aromatic ring in benzaldehyde for **SB 1** to **SB 10** are 2-OH, 3-OH, 4-OH, 2-

Cl, 4-Cl, 2,4-Cl_2, H, 4-CH_3, 4-OCH_3, and 4-NO_2, respectively. The obtained yields ranged from 67% to 96%.

In general, most compounds exhibited the yields above 70%, except for the **SB 7**, which showed a slightly lower yield of 67%. This may be attributed to the absence of electron-donating or electron-withdrawing substituents on the benzaldehyde ring, resulting in lower reactivity. Compounds bearing electron-withdrawing groups (EWGs) such as 2-Cl, 4-Cl, 2,4-Cl_2, and 4-NO_2 tend to give higher yields compared to those containing electron-donating groups (EDGs) like 2-OH, 3-OH, 4-OH, and 4-OCH_3. This is because EWGs increase the electrophilicity of the carbonyl carbon, thereby facilitating nucleophilic attack by the hydrazide (Badawy *et al*., 2025). However, an exception is observed for the 4-CH_3 substituted derivative (**SB 8**), where the yield remains relatively high despite being an EDG. This may be due to its weaker electron-donating effect and minimal steric hindrance, which does not significantly reduce the reactivity of the carbonyl group.

Melting point determination is a reliable method for purity assessment (Moondra *et al*., 2018). The melting points of the synthesised *N*-acylhydrazones **SB 1**- **SB 10** lie between the temperature range of °C, with narrow melting intervals of approximately 2–3 °C. Such sharp ranges indicate a high degree of purity. As even small amounts of impurities can lower the melting point value of a compound and broaden the range due to eutectic behaviour (Alexander , 2019; Darsaklis, 2025).

Most of the products were obtained as dark brown, brown, or light brown solids. An exception was **SB 10,** which appears as a light orange solid, likely due to the presence of the strongly electron-withdrawing nitro (NO_2) group. By lowering the energy of the molecular orbitals, particularly the LUMO, the nitro group facilitates electronic transitions at lower energy (Farley *et al*., 2018). As a result, absorption is shifted from the ultraviolet region into the visible region, leading to the appearance of colour. Nitro compounds are therefore typically yellow to orange because the $–NO_2$ group acts as a strong chromophore that extends conjugation and alters electron distribution, enabling absorption of visible light and giving rise to the observed light orange colour (Kumar *et al*., 2021).

An ethyl acetate:hexane (1:1) solvent system was used in Thin-layer chromatography (TLC) analysis, yielding a retardation factor (R_f) of 0.04-0.43. Most compounds showed R_f values around 0.10, except for **SB 3**, which exhibited the lowest value (0.04). This low R_f value can be attributed to the compound's relatively high polarity, owing to the presence of the *para* positions of the hydroxyl (4’-OH) group, which enhances interactions with the polar silica gel stationary phase of the TLC plate, thereby resulting in stronger retention of **SB 3**. As a result, the compound was more strongly retained and migrated more slowly, remaining closer to the baseline. More polar compounds interact more strongly with the silica; they are less likely to be displaced by the mobile phase, causing them to migrate more slowly and stay closer to the baseline (Bele *et al*., 2011). The physical properties of *N*-acylhydrazones **SB 1–SB 10** are

summarized in **Table 4.4**.

Table 4.4: Physicochemical properties of *N*-acylhydrazones **SB 1-SB 10**

4.4.2 IR Characterizations of *N*-acylhydrazones SB 1-SB 10

The presence of functional groups in the synthesized *N*-acylhydrazones (**SB 1-SB 10**) was verified by the FTIR spectral data (**Figures 4.12** to **4.21**). The aromatic sp^2 C-H stretches appearing around 3042-3066 cm^{-1} was observed. Additionally, the sharp aromatic C=C stretching was found to be in the range of 1606-1558 cm^{-1}. For the *N*-acylhydrazone moiety, strong C=O stretching was observed at 1669-1654 cm^{-1}, and C=N stretches were seen around 1651-1587 cm^{-1}, accompanied by a weaker C-N stretch at 1077-1033 cm^{-1}. The peak of the imine bond (C=N) is observed, indicating the formation of the *N*-acylhydrazone.. Such broadening is often due to hydrogen bonding interactions, as well as overlapping signals from traces of water or C-H stretching vibrations, which can influence the clarity of the N-H peak (Hansen *et al*., 2021). For the sp^3 C-H stretches, attributed to methyl (CH_3) and methylene (CH_2) groups, appeared between 2916-2878 cm^{-1}. In the compounds of **SB 1**, **SB 2** and **SB 3**, which contained hydroxyl (OH) groups, showed O-H stretches at 3182, 3301, and 3281 cm^{-1}, respectively, which falls within the characteristic FTIR absorption literature reported literature value for hydroxyl groups (Mirfazli *et al*., 2014). **SB 4**, **SB 5**, and **SB 6**, which contained the chlorine (Cl) atom, the C–Cl stretching

vibrations are present at 796, 797, and 786 cm^{-1}, respectively, which falls within the characteristic range of ~800–700 cm^{-1} for aromatic C–Cl (Nandiyanto *et al*., 2023). **SB 9**, which contained a methoxy (OCH_3) group, displayed a distinct C-O-C stretching vibration around 1252 cm^{-1}, characteristic of the ether bond in the methoxy group and this absorption was consistent with the typical stretching vibration of C-O-C in methoxy-substituted aromatic compounds (Zhang *et al*., 2022). The nitro (NO_2) group in **SB 10** exhibited distinctive N-O stretches at 1520 cm^{-1} (asymmetric) and 1341 cm^{-1} (symmetric), which aligns with the typical absorption ranges of 1520–1550 cm^{-1} for the asymmetry stretching and 1340–1380 cm^{-1} for the symmetry stretching (Chaudhary, 2025).

The IR spectral data for *N*-acylhydrazones **SB 1**– **SB 10** are summarized in **Table 4.5**.

Table 4.5: Summary of FTIR spectral data for *N*-acylhydrazones **SB1** – **SB10**

Figure 4.12: FT-IR (KBr, cm^{-1}) spectrum of *N*-acylhydrazone **SB 1**

Figure 4.13: FT-IR (KBr, cm^{-1}) spectrum of *N*-acylhydrazone **SB 2**

Figure 4.14: FT-IR (KBr, cm-1) spectrum of N-acylhydrazone **SB 3**

Figure 4.15: FT-IR (KBr, cm^{-1}) spectrum of *N*-acylhydrazone **SB 4**

Figure 4.16: FT-IR (KBr, cm^{-1}) spectrum of *N*-acylhydrazone **SB 5**

Figure 4.17: FT-IR (KBr, cm^{-1}) spectrum of *N*-acylhydrazone **SB 6**

Figure 4.18: FT-IR (KBr, cm^{-1}) spectrum of *N*-acylhydrazone **SB 7**

Figure 4.19: FT-IR (KBr, cm^{-1}) spectrum of *N*-acylhydrazone **SB 8**

Figure 4.20: FT-IR (KBr, cm^{-1} spectrum of *N*-acylhydrazone **SB 9**

Figure 4.21: FT-IR (KBr, cm^{-1}) spectrum of *N*-acylhydrazone **SB 10**

4.4.3 NMR Structural Characterizations of *N*-acylhydrazones

A total of ten *N*-acylhydrazones (**Figure 4.22)** were synthesized, and their chemical structure were characterized through a range of NMR spectroscopy techniques. The data obtained from ^{1}H NMR, ^{13}C NMR, DEPT 135, HMQC, and HMBC spectra provided structural information, thereby confirming the formation of synthesized *N*-acylhydrazones **SB 1**-**SB 10**.

Figure 4.22: General structure and Numbering of Compounds **SB 1**-**SB 10**

The synthesized *N*-acylhydrazones exhibited both geometrical and conformational isomerism, resulting from the restricted rotation of the imine (C=N) bond and the rotation around the C–N single bond of the amide linkage (Munir *et al*., 2021). However, only the *E* isomer of *N*-acylhydrazones were synthesized. Conformational isomerism existed in the form of both synperiplanar (*syn*) and antiperiplanar (*anti*) conformers in all the synthesized compounds, as evidenced by duplication of signals observed in the ^{1}H and ^{13}C NMR spectra (Lopes *et al*., 2013).

To quantify the relative amounts of *syn* and *anti* conformers, the amide proton

(H-10) signals in the ^{1}H NMR spectrum were integrated. This approach has been used in previous studies of conformers, where the ratio of signals for each *syn* and *anti* conformer was obtained directly from their integral values in the NMR spectrum (Quintanilla Licea *et al*., 2002). In the *syn* form, the amide proton (H10) is perpendicular to the carbonyl double bond, which shields it and causes an upfield shift in the spectrum (Xue & Nestor, 2022). In contrast, the amide proton (H10) of the *anti* conformer was much more deshielded, causing it to appear further downfield compared to that of the *syn* conformer. Initially, the *syn* and *anti* signals of the amide proton were identified, thereby allowing differentiation of the remaining signals for both conformers based on their relative intensities.

Proton signals from the same conformer are expected to display consistent intensity ratios. For instance, if the proton of the *syn* conformer appears more intense, the other proton signals of the *syn* conformer will also exhibit greater intensities compared to those of the *anti* conformer. This correlation allows the quantification of the relative populations of each conformer (Pettitt *et al*., 2024). As the integrated peak areas reflect the conformer distribution within the compound.

Most of the synthesized compounds (**SB 2- SB 10**) exhibit a higher proportion of the *syn* conformer, as indicated by the greater intensity of the *syn* signals in the spectrum. However, an exception occurred in **SB 1**, which contains a hydroxyl group at position 2'. It showed a stronger *anti* signal than the *syn* signal, suggesting a higher proportion of the *anti* conformer. This observation indicated

that the presence of the hydroxyl group at the 2' position may shift the *syn*/*anti* equilibrium towards the *anti* form by stabilizing the *anti* conformer more than the *syn* conformer.

In the ^{1}H NMR spectrum, non-aromatic protons typically resonate in the upfield region, while protons attached to nitrogen are observed downfield due to the increased deshielding effect from the electronegativity of the nitrogen atom. The signals corresponding to the aromatic protons of the indole and benzaldehyde groups generally appear between 6.0 and 8.0 ppm (Zhu *et al*., 2018). Within each group, the indole protons (H-1) exhibit relatively consistent chemical shifts, reflecting their similar electronic environments, whereas the benzaldehyde aromatic protons show comparable shifts, depending on whether an electron-withdrawing or donating group is present in the benzaldehyde. This pattern allows easy identification and differentiation of protons within aromatic regions. A comparable pattern in chemical shifts is observed in the ^{13}C NMR spectrum.. Compound **SB 8** has been selected as the model in the discussion of the structure elucidation of *N*-acylhydrazones.

4.4.3.1 ^{1}H NMR Structural Characterizations of *N*-acylhydrazone SB 8

In the ^{1}H NMR spectrum of **SB 8** (**Figure 4.23**), a total of proton signals were observed, although having a total of protons. This is due to the plane of symmetry observed in the synthesized *N*-acylhydrazone **SB 8**, which causes H-2' and H-3'

to appear at the same chemical shift as H-6' and H-5', respectively.

In the downfield region, the signals at δ_{syn} /δ_{anti} corresponding to H, δ_{syn} /δ_{anti} for the H-1 and δ_{syn} /δ_{anti} corresponded to H.

The formation of the *N*-acylhydrazone can be confirmed by the presence of the imine proton in the ^{1}H NMR spectrum.

The H-12 proton, attached to the imine carbon, undergoes deshielding due to the imine double bond (C=N) and the adjacent electronegative nitrogen atom, which withdraws electron density (Ereminsoy *et al*., 2026). Additionally, the imine (C═N) π-bond creates a magnetic anisotropic field that further deshields nearby imine protons (Kennepohl, Farmer, and Spinney, 2016). This interaction with the external magnetic field caused the downfield shifts, placing the imine proton in the typical range for azomethine protons. While both the H-10 and H-1, which were the protons that attached to nitrogen atoms in the amide and indole groups, were observed further downfield in ^{1}H NMR spectrum because they experience greater deshielding effects and consequently appeared at higher chemical shifts than the imine proton (H-12). However, the amide NH (H-10) was more deshielded due to its proximity to the carbonyl group and the imine double bond, leading to greater electron-withdrawing effects. This increased deshielding effect makes the amide proton appear further downfield compared to the indole NH (H-1) proton.

After comparison with the spectrum obtained after the addition of D_2O, both the

amide –NH (H-10) and indole –NH (H-1) signals disappeared due to the rapid intermolecular exchange of proton with deuterium (Anthony, 2017, Dyson *et al*., 2009; Zhang *et al*., 1995).

Figure 4.23: ^{1}H NMR (400 MHz, DMSO-d_6) spectrum of **SB 8**

4.4.3.2 ^{13}C NMR Structural Characterizations of *N*-acylhydrazone SB 8

In the ^{13}C NMR spectrum (**Figure 4.24**) of **SB 8**, a total of signals were observed, although the compound contains a total of carbons. This is due to the plane of symmetry observed in the synthesized *N*-acylhydrazone **SB 8**, which causes C-2' and C-3' to appear at the same chemical shift as C-6' and C-5', respectively.

The carbon signals were further classified into methyl (CH_3), methylene (CH_2), methine (CH), and quaternary carbons based on the DEPT 135 experiment (Atta-ur-Rahman *et al*., 2016). In this spectrum, quaternary carbons were absent, methyl and methine carbons appear as a positive region, while methylene carbons appear in the negative region (Santos & Silva, 2014). The methyl carbon is more shielded compared to the methine carbons. Therefore, by comparison with the DEPT-135 spectrum and the ^{13}C NMR spectrum, a total of six quaternary carbons were identified.

Similarly, these assignments were further confirmed by the correlations in the HMQC and HMBC spectra. Hence, the formation of the *N*-acylhydrazone was confirmed by the presence of the imine carbon (C-12) in the ^{13}C NMR spectrum.

Through the HMQC (**Figure 4.25)** and HMBC (**Figure 4.26**) spectra, the correlations between protons and carbons can thus be revealed. As HMQC is a 2D-NMR technique that provides direct single-bond correlations between protons and their directly attached carbon atoms (Claridge, 2016). While HMBC

reveals long-range (around two to four-bond) $^{13}C–^{1}H$ correlations and provides connectivity information between neighbouring atoms (Agarwal *et al*., 2018).

Figure 4.24: ^{13}C NMR (100 MHz, DMSO-*d6*) spectrum of **SB 8**

Figure 4.25: HMQC NMR spectrum of **SB 8**

Figure 4.26: HMBC NMR spectrum of **SB 8**

4.4.3.3 NMR Structural Characterization of SB 8

The chemical structure of **SB 8** and a summary of its ^{1}H and ^{13}C NMR spectral data are presented in **Figure 4.27** and **Table 4.6**, respectively.

Figure 4.27: Chemical structure and Numbering of **SB 8**

Table 4.6: Summary of ^{1}H and ^{13}C NMR spectral data of **SB 8**

4.4.3.4 NMR Structural Characterization of SB 1

The chemical structure of **SB 1** and a summary of its ^{1}H and ^{13}C NMR spectral data are presented in **Figure 4.28** and **Table 4.7**, respectively. The ^{1}H NMR, ^{13}C NMR, HMQC, and HMBC spectra of **SB 1** are presented in the **Appendices**.

Figure 4.28: Chemical structure of **SB 1**

Table 4.7: Summary of ^{1}H and ^{13}C NMR spectral data of **SB 1**

4.4.3.4 NMR Structural Characterization of SB 2

The chemical structure of **SB 2** and a summary of its ^{1}H and ^{13}C NMR spectral data are presented in **Figure 4.29** and **Table 4.8**, respectively. The ^{1}H NMR, ^{13}C NMR, HMQC, and HMBC spectra of **SB 2** are presented in the **Appendices**.

Figure 4.29: Chemical structure of **SB 2**

Table 4.8: Summary of ^{1}H and ^{13}C NMR spectral data of **SB 2**

4.3.3.5 NMR Structural Characterization of SB 3

The chemical structure of **SB 3** and a summary of its ^{1}H and ^{13}C NMR spectral data are presented in **Figure 4.30** and **Table 4.9**, respectively. The ^{1}H NMR, ^{13}C NMR, HMQC, and HMBC spectra of **SB 3** are presented in the **Appendices**.

Figure 4.30: Chemical structure of **SB 3**

Table 4.9: Summary of ^{1}H and ^{13}C NMR spectral data of **SB 3**

4.3.3.6 NMR Structural Characterization of SB 4

The chemical structure of **SB 4** and a summary of its ^{1}H and ^{13}C NMR spectral data are presented in **Figure 4.31** and **Table 4.10**, respectively. The ^{1}H NMR, ^{13}C NMR, HMQC, and HMBC spectra of **SB 4** are presented in the **Appendices**.

Figure 4.31: Chemical structure of **SB 4**

Table 4.10: Summary of ^{1}H and ^{13}C NMR spectral data of **SB 4**

4.3.3.7 NMR Structural Characterization of SB 5

The chemical structure of **SB 5** and a summary of its ^{1}H and ^{13}C NMR spectral data are presented in **Figure 4.32** and **Table 4.11**, respectively. The ^{1}H NMR, ^{13}C NMR, HMQC, and HMBC spectra of **SB 5** are presented in the **Appendices**.

Figure 4.32: Chemical structure of **SB 5**

Table 4.11: Summary of ^{1}H and ^{13}C NMR spectral data of **SB 5**

4.3.3.8 NMR Structural Characterization of SB 6

The chemical structure of **SB 6** and a summary of its ^{1}H and ^{13}C NMR spectral data are presented in **Figure 4.33** and **Table 4.12**, respectively. The ^{1}H NMR, ^{13}C NMR, HMQC, and HMBC spectra of **SB 6** are presented in the **Appendices**.

Figure 4.33: Chemical structure of **SB 6**

Table 4. 12: Summary of ^{1}H and ^{13}C NMR spectral data of **SB 6**

4.3.3.9 NMR Structural Characterization of SB 7

The chemical structure of **SB 7** and a summary of its ^{1}H and ^{13}C NMR spectral data are presented in **Figure 4.34** and **Table 4.13**, respectively. The ^{1}H NMR, ^{13}C NMR, HMQC, and HMBC spectra of **SB 7** are presented in the **Appendices**.

Figure 4.34: Chemical structure of **SB 7**

Table 4. 13: Summary of ^{1}H and ^{13}C NMR spectral data of **SB 7**

4.4.3.10 NMR Structural Characterization of SB 9

The chemical structure of **SB 9** and a summary of its ^{1}H and ^{13}C NMR spectral data are presented in **Figure 4.35** and **Table 4.14**, respectively. The ^{1}H NMR, ^{13}C NMR, HMQC, and HMBC spectra of **SB 9** are presented in the **Appendices**.

Figure 4.35: Chemical structure of **SB 9**

Table 4. 14: Summary of ^{1}H and ^{13}C NMR spectral data of **SB 9**

4.4.3.11 NMR Structural Characterization of SB 10

The chemical structure of **SB 10** and a summary of its ^{1}H and ^{13}C NMR spectral data are presented in **Figure 4.36** and **Table 4.15**, respectively. The ^{1}H NMR, ^{13}C NMR, HMQC, and HMBC spectra of **SB 10** are presented in the **Appendices**.

Figure 4.36: Chemical structure of **SB 10**

Table 4. 15: Summary of ^{1}H and ^{13}C NMR spectral data of **SB 10**

4.5.4 Isomerism Studies of *N*-acylhydrazones

N-acylhydrazones, which contain both the amide [C(=O)-NH] and imine (C=N) functional groups, give rise to both conformational (*syn*/*anti*) and geometric (*E*/*Z*) isomerism. In fact, *N*-acylhydrazones should exist in four distinct isomers, which include both the *syn*/*anti* conformers and *E* and *Z* geometrical isomers, as shown in **Figure 4.37** (Socea *et al*., 2022). However, research by Munir *et al*. (2020) has shown that *N*-acylhydrazones predominantly exist as mixtures of *syn*/*anti* conformers of the *E* isomer, as evidenced by NOE experiments. The preference for the *E* isomer was owing to its greater stability, which results in less steric repulsion than in the *Z* isomer.

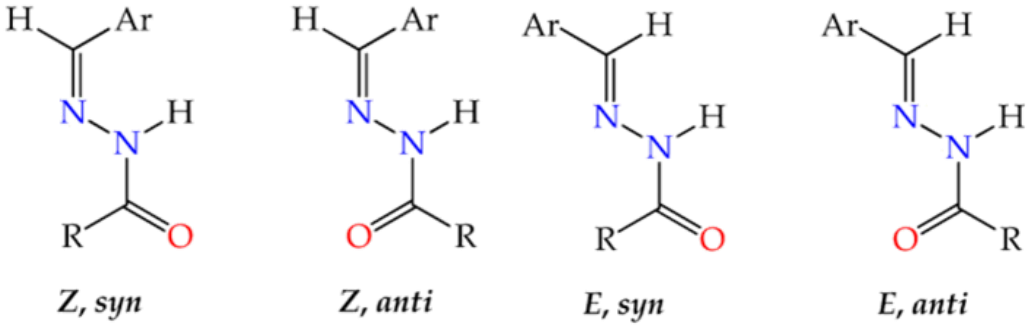

Figure 4.37: Possible Isomers of *N*-acylhydrazone Derivatives

4.5.4.1 Conformation of CO-NH bond of *N*-acylhydrazones

The relative population of the *syn*/*anti* amide conformers was quantified by analyzing the integration values of their corresponding peaks in the ^{1}H NMR spectrum. In this study, the integration value of the amide proton (H-10), which was attached to the nitrogen in amide group (CO-NH), was used to calculate the conformer percentage due to its prominent downfield signal and has been extensively confirmed in various studies (O'Callaghan *et al*., 2001; Pettitt *et al*., 2024; Quintanilla-Licea *et al*., 2002; Xue and Nestor, 2022). In addition, the amide proton of the *syn* conformer appeared more intense (higher intensities) compared to those of the *anti* conformer. Again, the amide proton of the *anti* conformer was much more deshielded, resulting in a further downfield signal compared to that of the *syn* conformer. According to **Table 4.16**, most of the synthesized compounds (**SB 2**–**SB 10)** exhibited a higher proportion of the *syn* conformer than the *anti* conformer, as indicated by the stronger intensity of the

syn signals. However, an exception was observed in **SB 1**, which contains a hydroxyl group at the *ortho* position (2'-OH), and the reason will be discussed in detail later.

Figure 4.38: ^{1}H NMR spectrum of **SB 8**, Amide N-H region, and integration

Based on the integration values shown in **Figure 4.38**, the *syn* conformer has an integration value of 1.00, while the *anti* conformer has an integration value of 0.72. The percentages of the *syn* and *anti* conformers can therefore be calculated using the following formula.

$$\%\ syn = \frac{syn}{syn+anti} \times 100\% \qquad \%\ anti = \frac{anti}{syn+anti} \times 100\%$$

The percentages of *syn* and *anti* conformers of **SB 1**-**SB 10** were summarized in Table **4.16**.

Table 4.16: Summary of the percentages of *syn*/*anti* conformers of **SB 1-SB 10**

Figure 4.39: Chemical Structures of the *syn* and *anti* conformers of **SB 1**

SB 1 predominantly exists in the *anti* conformation rather than the *syn* is because the *ortho*-hydroxyl (2'-OH) group of the compound is positioned closer to the amide carbonyl oxygen compared to the *syn* conformer in the *anti* conformation (**Figure 4.39**). Hence, enabling the formation of a strong intramolecular

hydrogen bond. This interaction stabilizes the *anti* conformer by restricting the rotational freedom and provides greater stability against conformational changes (Ali *et al*., 2025). In contrast, the *syn* conformer lacks the appropriate geometry for such hydrogen bonding, making it less stable than the *anti* conformer. Consequently, the *anti* conformer predominates over the *syn* conformer.

4.5.4.2 Geometric Isomerism of *N*-acylhydrazones

To assess the geometrical isomerism of *N*-acylhydrazones formed by the restricted rotation around the imine (C=N) bond, Differential Nuclear Overhauser Effect (NOE) experiments were conducted, with **SB 8** chosen as an example. The differential NOE spectra of **SB 8** (**Figures 4.40)** showed that irradiation at δ, corresponding to the amide proton (H), led to a % NOE enhancement of the imine proton (H) at δ. Similarly, when the imine proton (H) at δ was irradiated **(Figure 4.41**), NOE enhancements with % and % were observed for the amide proton (H), and aromatic proton (H) of benzaldehyde at δ1 and δ7, correspondingly. Similar observations were also observed for other synthesized *N*-acylhydrazones. Based on these NOE_{diff} spectra, only the *E* isomer showed such NOE enhancements, whereas the *Z* isomer did not. As irradiation of the amide proton (H-1) in the *E* isomer enhanced the imine proton (H-12), but this effect was absent in the *Z* isomer (Lopes *et al*., 2013). Therefore, the NOE results strongly aligned with the presence of greater stability of the *E*

isomer in the compounds **SB 1** to **SB 10**.

Figure 4.40: Differential NOE spectrum of **SB 8**, irradiated amide proton (H10)

Figure 4.41: Differential NOE spectrum of **SB 8**, irradiated imine proton (H12)

4.5.4.3 Rotational Barriers around the CO-NH Bond for *N*-acylhydrazones

Dynamic NMR experiments were performed to investigate the energy rotational barriers or Gibbs free energy of activation between the *syn* and *anti* conformers of the synthesized *N*-acylhydrazones (Hamzi, Barhoumi-Slimi and Abidi, 2016). Compound **SB 8** was selected as a representative example for this analysis. As the temperature increased, the coalescence was observed at the coalescence temperature (T_c), as shown in the dynamic NMR spectrum (**Figure 4.42**).

Figure 4.42: Dynamic NMR Spectrum of **SB 8**

To determine the Gibbs free energy of activation, the coalescence temperature (T_c) of the amide proton (H10) peak for the compound **SB 8** was first identified as 90°C. Which was then converted to Kelvin by adding 273.15 K, resulting in a temperature of 363.15 K. Next, the rate constant (k_c) which is the rate of exchange between the *syn* and *anti* conformers was determined by measuring the peak separation (Δν, in Hz) between the *syn* and *anti* conformer of amide proton (H10) at a temperature below the coalescence temperature, as observed in the dynamic NMR spectrum. Converting the peak separation Δν from ppm to hertz units is achieved by multiplying the chemical shift in ppm by the NMR spectrometer's operating frequency in MHz. After obtaining the T_c and Δν, the rate constant (k_c) can be thus calculated using the following equation: $k_c = (\pi \times \Delta\nu)/\sqrt{2}$.

According to Hamzi, Barhoumi-Slimi and Abidi (2016), by rearranging the Eyring equation, the formula for calculating the Gibbs free energy of activation can thereby be derived: $\Delta G^{\ddagger} = 19.14T_c\,(10.32 + \log \frac{T_c}{k_c}) \times 10^{-3}$. Consequently, the rotational energy barrier can thus be determined. The Gibbs free energies of activation for compounds **SB 1- SB 10** were summarized in **Table 4.17**.

Table 4.17: Summary of the Gibbs free energy of activation of **SB 1- SB 10**

The energy of activation $\Delta G^{\neq}$ of all the synthesized *N*-acylhydrazone **SB 1-SB 10** fell within a relatively narrow range, from 73.47 to 77.81 kJ/mol, indicating that they exhibit similar rotational barriers. This similarity in rotational barriers suggests that the compounds undergo similar conformational changes and exchange rates.

Figure 4.43: Comparison of ^{1}H NMR spectrum of **SB 8** at 21 ℃ and 100℃

At room temperature (21°C), the C–N bond of the amide group exhibits partial double-bond character due to resonance, which restricts rotation around the bond and results in slow rotation (Lopes *et al*., 2013). As a consequence, both the *syn* and *anti* conformers are observable in the NMR spectrum. However, at higher temperatures (100°C), the molecules gain kinetic energy, causing the rotation around the C–N bond to become less restricted and thereby rotate faster. This leads to rapid interconversion between the *syn* and *anti* conformers, and the NMR can no longer distinguish them separately. Consequently, the signals average out, leading to coalescence in which the separate peaks merge into a single peak. This produced a broad singlet peak, in contrast to the distinct two singlet peaks observed at room temperature (21°C) (**Figure 4.43**).

CHAPTER 5

CONCLUSION

5.1 Conclusion

A total of ten *N*-acylhydrazone derivatives (**SB 1**-**SB 10**) bearing an indole moiety were synthesized through the condensation reaction between carboxylic acid hydrazide and a series of substituted benzaldehydes. The yields of the compounds ranged from 67% to 96%. Characterization was carried out using various techniques, including physical observations (color and solid physical state), melting-point analysis, and various spectroscopic methods: FTIR, ^{1}H NMR, ^{13}C NMR, DEPT 135, HMQC, and HMBC. The *E*/*Z* isomerism of the synthesized *N*-acylhydrazone derivatives were confirmed using differential NOE experiments with irradiation at both the amide (H10) and imine proton (H12). The findings revealed that all synthesized *N*-acylhydrazone derivatives predominantly exist as the *E* isomer, as determined from NOE results. For compounds **SB 2**-**SB 10**, the percentages of *syn* and *anti* conformers were 58 and 40, respectively. However, **SB 1** showed a higher proportion of the *anti* conformer, with *syn* and *anti* conformers. Most of the compounds existed

predominantly in the *syn* conformer, exclusion for **SB 1**, which displayed a higher proportion of the *anti* conformer. To assess the rotational barrier between the two conformers, dynamic NMR experiments were performed, yielding Gibbs free energy of activation values ranging between 6 kJ/mol and 7 kJ/mol.

5.2 Further Studies

N-acylhydrazone derivatives exhibit a variety of pharmacological activities, including anti-inflammatory, antimicrobial, antibacterial, anticancer, cytotoxic, and other properties (Socea *et al*., 2022). These promising biological activities make them an attractive candidate for further study. Mass spectrometry can be used to determine the mass-to-charge ratios of both their molecular ions and fragment ions. This provides the molecular weight, thereby allowing determination of the molecular formula and structural information from fragment ions (Ma, 2022). Furthermore, elemental CHN analysis can quantitatively determine the presence and mass percentages of carbon (C), hydrogen (H), and nitrogen (N), providing essential information about their elemental composition (Elżbieta Frąckowiak *et al*., 2022). Additionally, molecular docking studies can be conducted to investigate the interactions of *N*-acylhydrazones with various target proteins (Mikus *et al*., 2023).

REFERENCES

Abdel-Aziz, H.A. *et al*. (2013) 'The reaction of ethyl 2-oxo-2H-chromene-3-carboxylate with hydrazine hydrate', *Molecules*, 18(2), pp. 2084–2095. Available at: https://doi.org/10.3390/molecules18022084.

Aboonajmi, J. *et al*. (2015) 'Tartaric acid: a natural, green and highly efficient catalyst for the one-pot synthesis of functionalized piperidines', *Research on Chemical Intermediates*, 41(11), pp. 8057–8065. Available at: https://doi.org/10.1007/s11164-014-1877-1.

Abraham, R.J. *et al*. (2000) 'Proton chemical shifts in NMR. Part 14. Proton chemical shifts, ring currents and π electron effects in condensed aromatic hydrocarbons and substituted benzenes', *Journal of the Chemical Society Perkin Transactions 2*, (4), pp. 803–812. Available at: https://doi.org/10.1039/a907830d.

Acquisto, N.M. (2014) 'Isoniazid', *Encyclopedia of Toxicology*, pp. 1135–1137. Available at: https://doi.org/10.1016/B978-0-12-386454-3.00740-5.

Agarwal, N. *et al*. (2018) 'Characterization of nanomaterials using nuclear magnetic resonance spectroscopy', *Characterization of Nanomaterials: Advances and Key Technologies*, pp. 61–102. Available at: https://doi.org/10.1016/B978-0-08-101973-3.00003-1.

Agili, F. (2024) ‘Novel hydrazide hydrazone derivatives as antimicrobial agents: design, synthesis, and molecular dynamics’, *Processes*, 12(6), p. 1055. Available at: https://doi.org/10.3390/pr12061055.

Alexander, S. (2019). *5.3: Melting Point Analysis- Identity and Purity*. Available at: https://chem.libretexts.org/Bookshelves/Organic_Chemistry/Book%3A_How_to_be_a_Successful_Organic_Chemist_%28Sandtorv%29/05%3A_HOW_TO_INTERPRET_YOUR_RESULTS/5.03%3A_MELTING_POINT_ANALYSIS-_IDENTITY_AND_PURITY (Accessed 17 Apr. 2026).

Ali, M.I. *et al*. (2025) ‘Intramolecular noncovalent C-bonding driven conformational preference in spiroisatin-based *N*-acyl hydrazones’, *RSC Advances*, 15(2), pp. 1152–1162. Available at: https://doi.org/10.1039/D4RA08086F.

Anthony, F. (2017) “On NH chemical shifts, Part V: NH and NH_2 chemical shifts of hydrazides and related compounds.,” *Molecules*, 16(5), pp. 3544–3551. Available at: https://doi.org/10.3390/molecules16053544.

Antoniolli, G. *et al*. (2026) ‘*N*-Acylhydrazones: applications and advances in drug discovery’, *European Journal of Medicinal Chemistry Reports*, 16, p.

100317. Available at: https://doi.org/10.1016/j.ejmcr.2025.100317.

Atta-ur-Rahman, Choudhary, M.I. and Atia-tul-Wahab. (2016) 'Chapter four - spin-echo and polarization transfer', in Elsevier (eds) *Solving Problems with NMR Spectroscopy*, pp. 133–190. Available at: https://doi.org/10.1016/B978-0-12-411589-7.00004-8.

Badawy, S.A. *et al*. (2025) 'Novel triazole-carbohydrazide hydrazones with dual antioxidant and antibacterial potential', *Scientific Reports*, 15(1), p. 41456. Available at: https://doi.org/10.1038/S41598-025-26016-X.

Bayer, E.A., Ben-Hur, H. and Wilchek, M. (1988) 'Biocytin hydrazide—a selective label for sialic acids, galactose, and other sugars in glycoconjugates using avidin-biotin technology', *Analytical Biochemistry*, 170(2), pp. 271–281. Available at: https://doi.org/10.1016/0003-2697(88)90631-8.

Bele, A.A. *et al*. (2011) 'An overview on thin layer chromatography', *IJPSR*, 2(2), pp. 256–267. Available at: https://doi.org/https://dx.doi.org/10.13040.

Biliz, Y. *et al*. (2023) 'Novel *N*-Acylhydrazone compounds as promising anticancer agents: synthesis and molecular docking studies', *ACS Omega*, 8(22), pp. 20073–20084. Available at: https://doi.org/10.1021/acsomega.3c02361.

Bradley, D. *et al*. (2023) ‘Disentangling global and local ring currents’, *Chemical Science*, 14(7), pp. 1762–1768. Available at: https://doi.org/10.1039/D2SC05923A.

Çelebi-Ölçüm, N. *et al*. (2011) ‘Why do some Fischer indolizations fail’, *Journal of the American Chemical Society*, 133(15), pp. 5752–5755. Available at: https://doi.org/10.1021/ja201035b.

Chaloupecká, E. *et al*. (2024) ‘Exploring long-range fluorine–carbon *J*-coupling for conformational analysis of deoxyfluorinated disaccharides: A combined computational and NMR study’, *Bioorganic Chemistry*, 147, p. 107388. Available at: https://doi.org/10.1016/j.bioorg.2024.107388.

Chang, J. *et al*. (2023) ‘A comprehensive investigation of hydrazide and its derived structures in the agricultural fungicidal field’, *Journal of Agricultural and Food Chemistry*, 71(22), pp. 8297–8316. Available at: https://doi.org/10.1021/acs.jafc.3c00786.

Chaudhary, J. (2025) ‘FTIR spectroscopic analysis of pyrimidine derivatives: a comprehensive review’, *Applied Science and Biotechnology Journal for Advanced Research*, (2), pp. 1–5. Available at: https://doi.org/10.5281/zenodo.15369611.

Claridge, T.D.W. (2016) ‘Correlations through the chemical bond II: heteronuclear shift correlation’, *High-Resolution NMR Techniques in Organic Chemistry*, pp. 243–294. Available at: https://doi.org/10.1016/B978-0-08-099986-9.00007-5.

Cloutier, F. *et al.* (2025) ‘Exploring the synthesis, anti-Inflammatory and anti-tumor potential of 4-maleimidylphenyl-hydrazide derivatives’, *Molecules*, 30(20), p. 4035. Available at: https://doi.org/10.3390/molecules30204035.

Cordeiro, N.M. *et al*. (2016) ‘Discovery of novel orally active tetrahydro-naphthyl-*N*-Acylhydrazones with in Vivo anti-TNF-α effect and remarkable anti-Inflammatory properties’, *Plos One*, 11(5), p. e0156271. Available at: https://doi.org/10.1371/journal.pone.0156271.

Darsaklis, I. (2025) ‘Identification of an unknown organic compound by determination of its melting point’, *International Journal of Scientific Research in Chemical Sciences*, 12(1), pp. 28–32. Available at: https://doi.org/10.26438/IJSRCS.V12I1.184.

Dyson, H.J. *et al*. (2009) ‘Hydrogen–deuterium exchange strategy for delineation of contact sites in protein complexes’, *FEBS Letters*, 582(10), pp. 1495–1500. Available at: https://doi.org/10.1016/j.febslet.2008.03.043.

Edgar, M. *et al.* (2019) 'NMR spectral analysis of second-order ^{19}F-^{19}F, ^{19}F-^{1}H and ^{13}C-^{19}F coupling constants in pentafluorobenzene and tetrafluoro-4-(morpholino)pyridine using ANATOLIA', *Journal of Fluorine Chemistry*, 224, pp. 35–44. Available at: https://doi.org/10.1016/j.jfluchem.2019.04.018.

El-Sayed, M., Mahmoud, K. and Hilgeroth, A. (2014) 'Glacial acetic acid as an efficient catalyst for simple synthesis of dindolylmethanes', *Current Chemistry Letters*, 3(1), pp. 7–14. Available at: https://doi.org/10.5267/j.ccl.2013.10.003.

Elżbieta Frąckowiak *et al*. (2022) 'Chapter five - advanced characterization techniques for electrochemical capacitors', in van E. Rudi and D.H. Colin (eds.) *Advances in Inorganic Chemistry*, pp. 151–207. Available at: https://doi.org/10.1016/bs.adioch.2021.12.006.

Ereminsoy, E. *et al*. (2026) 'Synthesis, characterization, and lipoxygenase inhibition of salicylaldehyde-derived schiff base metal complexes: enzymatic and in silico evaluation using quinoa lipoxygenase', *Naunyn-Schmiedeberg's Archives of Pharmacology*, 399(6), pp. 8975–8990. Available at: https://doi.org/10.1007/s00210-025-04955-6.

Farley, C. *et al*. (2018) 'A structural model of nitro-porphyrin dyes based on spectroscopy and density functional theory', *Journal of Computational*

Chemistry, 39(18), pp. 1129–1142. Available at: https://doi.org/10.1002/jcc.24887.

Farmer , S., Soderberg , T. and Schaller, C.P. (2016). *13.5: Characteristics of ^{13}C NMR Spectroscopy*. Available at: https://chem.libretexts.org/Courses/Athabasca_University/Chemistry_350%3A_Organic_Chemistry_I/13%3A_Structure_Determination-_Nuclear_Magnetic_Resonance_Spectroscopy/13.05%3A_Characteristics_of_C_NMR_Spectroscopy (Accessed 14 April 2026).

Gautam, Y. *et al.* (2024) "Chapter 5 - Indoles: A Potential Drug Development Scaffold," *Multidisciplinary Approach and Applications of Material Science*, pp. 1–22.

Hamzi, I., Barhoumi-Slimi, T.M. and Abidi, R. (2016) 'Synthesis, characterization, and conformational study of acylhydrazones of α,β-unsaturated aldehydes', *Heteroatom Chemistry*, 27(3), pp. 139–148. Available at: https://doi.org/10.1002/hc.21310.

Hansen, P.E. *et al*. (2021) 'NH stretching frequencies of intramolecularly hydrogen-bonded systems: an experimental and theoretical study', *Molecules*, 26(24), p. 7651. Available at: https://doi.org/10.3390/molecules26247651.

Heravi, M.M. *et al*. (2021) 'Synthesis of indole derivatives as prevalent moieties present in selected alkaloids', *RSC Advances*, 11(53), pp. 33540–33612. Available at: https://doi.org/10.1039/D1RA05972F.

Hermanson, G.T. (2013) '(Strept)avidin–Biotin Systems', in Elsevier (3rd ed) *Bioconjugate Techniques*, pp. 465–505. Available at: https://doi.org/10.1016/B978-0-12-382239-0.00011-X.

Ibrahim, M.F. *et al*. (2013) 'Nucleophilic substitution reactions of 2,4-dinitrobenzene derivatives with hydrazine: leaving group and solvent effects', *International Journal of Chemistry*, 5(3). Available at: https://doi.org/10.5539/ijc.v5n3p33.

Inman, M. and Moody, C.J. (2013) 'Indole synthesis – something old, something new', *Chemical Science*, 4(1), pp. 29–41. Available at: https://doi.org/10.1039/C2SC21185H.

Kanabalan, R.D. *et al*. (2021) 'Human tuberculosis and Mycobacterium tuberculosis complex: A review on genetic diversity, pathogenesis and omics approaches in host biomarkers discovery', *Microbiological Research*, 246, p. 126674. Available at: https://doi.org/10.1016/j.micres.2020.126674.

Kaushik, Nagendra *et al*. (2013) 'Biomedical importance of indoles', *Molecules*, 18(6), pp. 6620–6662. Available at: https://doi.org/10.3390/molecules18066620.

Kennepohl, D., Farmer, S. and Spinney , R. (2016). *12.3: Chemical Shifts and Shielding.* Available at: https://chem.libretexts.org/Bookshelves/Organic_Chemistry/Map%3A_Organic_Chemistry_%28Wade%29_Complete_and_Semesters_I_and_II/Map%3A_Organic_Chemistry_%28Wade%29/12%3A_Nuclear_Magnetic_Resonance_Spectroscopy/12.03%3A_Chemical_Shifts_and_Shielding (Accessed 19 Apr. 2026).

Kumar, A., Dixit, U., Singh, K., Gupta, S.P., *et al*. (2021) 'Structure and properties of dyes and pigment', *Dyes and Pigments - Novel Applications and Waste Treatment*. Available at: https://doi.org/10.5772/INTECHOPEN.97104.

Kumar, A., Jakhar, A. and Makrandi, J.K. (2012) 'A highly efficient solvent free synthesis of hydrazides using grinding technique', in V. Gupta (ed.) *Heterocyclic Letters*, pp. 401–404. Available at: https://doi.org/https://heteroletters.org/.

Kumar, P. *et al*. (2017) 'Design, synthesis, conformational and molecular docking study of some novel acyl hydrazone based molecular hybrids as antimalarial and antimicrobial agents', *Chemistry Central Journal*, 11(1), p. 115. Available at: https://doi.org/10.1186/s13065-017-0344-7.

Kumar, S. and Ritika (2020) ‘A brief review of the biological potential of indole derivatives’, *Future Journal of Pharmaceutical Sciences*, 6(1). Available at: https://doi.org/10.1186/s43094-020-00141-y.

Lawrence, M.A.W. *et al*. (2019) ‘Review: voltammetric properties and applications of hydrazones and azo moieties’, *Polyhedron*, 173, p. 114111. Available at: https://doi.org/10.1016/j.poly.2019.114111.

Li, J. *et al*. (2019) ‘Indole compounds with *N*-ethyl morpholine moieties as CB2 receptor agonists for anti-inflammatory management of pain: synthesis and biological evaluation’, *Medicinal Chemistry Communications*, 10(11), pp. 1935–1947. Available at: https://doi.org/10.1039/C9MD00173E.

Li, M. *et al*. (2023) ‘Grape tartaric acid: chemistry, function, metabolism, and regulation’, *Horticulturae*, 9(11), p. 1173. Available at: https://doi.org/10.3390/horticulturae9111173.

Lim, J.Y., Sim, K.M. and Teo, K.C. (2025) ‘Antibacterial activity of 5-bromo substituted phenyl *N*-acylhydrazone derivatives with aromatic substitution at ortho- and para- directors as potential adjuvants’, *BIO Web of Conferences*, 182, p. 02008. Available at: https://doi.org/10.1051/bioconf/202518202008.

Lopes, A. *et al*. (2013) 'Characterization of amide bond conformers for a novel heterocyclic template of *N*-acylhydrazone derivatives', *Molecules*, 18(10), pp. 11683–11704. Available at: https://doi.org/10.3390/molecules181011683.

Lucas, S. (2016) 'The pharmacology of Indomethacin', *Headache: The Journal of Head and Face Pain*, 56(2), pp. 436–446. Available at: https://doi.org/10.1111/head.12769.

Ma, X. (2022) 'Recent advances in mass spectrometry-based structural elucidation techniques', *Molecules*, 27(19), p. 6466. Available at: https://doi.org/10.3390/molecules27196466.

Martin, N.H. *et al*. (2003) 'An NMR shielding model for protons above the plane of a carbonyl group', *Journal of Molecular Graphics and Modelling*, 22(2), pp. 127–131. Available at: https://doi.org/10.1016/S1093-3263(03)00152-9.

Mathada, B.S. *et al*. (2021) 'An insight into the advanced synthetic recipes to access ubiquitous indole heterocycles', *Tetrahedron Letters*, 85, p. 153458. Available at: https://doi.org/10.1016/j.tetlet.2021.153458.

Matsumoto, K. *et al*. (2003) 'Fischer indole synthesis in the absence of a solvent', *Heterocyclic Communications*, 9(1), pp. 9–12. Available at:

https://doi.org/10.1515/HC.2003.9.1.9.

Mikus, J. *et al*. (2023) 'Synthesis, biological, spectroscopic and computational investigations of novel *N*-acylhydrazone derivatives of Pyrrolo[3,4-d]pyridazinone as Dual COX/LOX Inhibitors', *Molecules*, 28(14), p. 5479. Available at: https://doi.org/10.3390/molecules28145479.

Mirfazli, S.S. *et al*. (2014) '*N*-substituted indole carbohydrazide derivatives: Synthesis and evaluation of their antiplatelet aggregation activity', *DARU Journal of Pharmaceutical Sciences*, 22(1). Available at: https://doi.org/10.1186/s40199-014-0065-6.

Mo, X. *et al*. (2024) 'Indole derivatives: a versatile scaffold in modern drug discovery—an updated review on their multifaceted therapeutic applications (2020–2024)', *Molecules*, 29(19), p. 4770. Available at: https://doi.org/10.3390/molecules29194770.

Moondra, S. *et al*. (2018) 'Bulk level properties and its role in formulation development and processing', *Dosage Form Design Parameters*, 2, pp. 221–256. Available at: https://doi.org/10.1016/B978-0-12-814421-3.00006-3.

Munir, R. *et al*. (2021) "Synthesis of novel *N*-Acylhydrazones and their C-N/N-

N bond conformational characterization by NMR Spectroscopy', *Molecules*, 26(16), p. 4908. Available at: https://doi.org/10.3390/molecules26164908.

Nandiyanto, A.B.D., Ragadhita, R. and Fiandini, M. (2023) 'Interpretation of fourier transform infrared spectra (FTIR): a practical approach in the polymer/plastic thermal decomposition', *Indonesian Journal of Science and Technology*, 8(1), pp. 113–126. Available at: https://doi.org/10.17509/ijost.v8i1.53297.

O'Callaghan, C.N. *et al*. (2001) 'Spectral analysis of amide conformers (s-cis and s-trans) of *N*-isopropylidenehydrazinocarbonyl derivatives', *Journal of Chemical Research*, 11, pp. 453–456. Available at: https://doi.org/10.3184/030823401103168523.

Pai, K.N. and Bhat, K.S. (2026) 'An overview on synthetic aspects and biological activity profiles of hydrazone derivatives', *Discover Chemistry*, 3(1), pp. 1-50. Available at: https://doi.org/10.1007/S44371-025-00463-X.

Pettitt, A.J. *et al*. (2024) 'An integrative characterization of proline cis and trans conformers in a disordered peptide', *Biophysical Journal*, 123(21), pp. 3798–3811. Available at: https://doi.org/10.1016/j.bpj.2024.09.028.

Popiołek, Ł. (2016) ‘Hydrazide–hydrazones as potential antimicrobial agents: overview of the literature since 2010’, *Medicinal Chemistry Research*, 26(2), p. 287. Available at: https://doi.org/10.1007/S00044-016-1756-Y.

Popiołek, Ł. *et al*. (2018) ‘New hydrazide-hydrazones and 1,3-thiazolidin-4-ones with 3-hydroxy-2-naphthoic moiety: Synthesis, in vitro and in vivo studies’, *Biomedicine & Pharmacotherapy*, 103, pp. 1337–1347. Available at: https://doi.org/10.1016/j.biopha.2018.04.163.

Popiołek, Ł. and Biernasiuk, A. (2017) ‘Synthesis and investigation of antimicrobial activities of nitrofurazone analogues containing hydrazide-hydrazone moiety’*, Saudi Pharmaceutical Journal*, 25(7), pp. 1097–1102. Available at: https://doi.org/10.1016/j.jsps.2017.05.006.

Porcheddu, A. *et al*. (2022) ‘Mechanochemical Fischer indolisation: an eco-friendly design for a timeless reaction’, *Green Chemistry*, 24(12), pp. 4859–4869. Available at: https://doi.org/10.1039/D2GC00724J.

Quintanilla-Licea, R. *et al*. (2002) ‘NMR detection of isomers arising from restricted rotation of the C-N amide bond of N-formyl-o-toluidine and N,N’-bis-Formyl-o-tolidine’, *Molecules*, 7(8), pp. 662–673. Available at: https://doi.org/10.3390/70800662.

Robinson, B. (1963) 'The Fischer Indole Synthesis', *Chemical Reviews*, 63(4), pp. 373–401. Available at: https://doi.org/10.1021/cr60224a003.

Sajjadifar, S. *et al*. (2010) 'New 3*H*-indole synthesis by Fischer's method. Part I', *Molecules*, 15(4), pp. 2491–2498. Available at: https://doi.org/10.3390/molecules15042491.

Salih, K. *et al*. (2020) 'Synthesis and pharmacological profile of some new 2-substituted-2, 3-dihydro-1H-perimidine', *Zanco Journal of Medical Sciences*, 24(1), pp. 68–79. Available at: https://doi.org/10.15218/zjms.2020.010.

Santos, C.M.M. and Silva, A.M.S. (2014) 'Nuclear magnetic resonance spectroscopy for structural characterization of bioactive compounds', *Comprehensive Analytical Chemistry*, 65, pp. 149–191. Available at: https://doi.org/10.1016/B978-0-444-63359-0.00007-0.

Sanz Sharley, D.D. and Williams, J.M.J. (2017) 'Acetic acid as a catalyst for the *N*-acylation of amines using esters as the acyl source', *Chemical Communications*, 53(12), pp. 2020–2023. Available at: https://doi.org/10.1039/C6CC09023K.

Schaller, C., Farmer, S., Kennepohl, D., Layne, M. and Soderberg, T. (2015). *13.11: DEPT ^{13}C NMR Spectroscopy*. Available at: https://chem.libretexts.org/Bookshelves/Organic_Chemistry/Organic_Chemistry_(Morsch_et_al.)/13%3A_Structure_Determination_-_Nuclear_Magnetic_Resonance_Spectroscopy/13.11%3A_DEPT_C_NMR_Spectroscopy (Accessed 22 Apr. 2026).

Shah, M.A. *et al*. (2022) 'Synthesis and characterization of novel hydrazone derivatives of isonicotinic hydrazide and their evaluation for antibacterial and cytotoxic potential', *Molecules*, 27(19), p. 6770. Available at: https://doi.org/10.3390/molecules27196770.

Shcherbakov, A.A. *et al*. (2020) 'Two-dimensional $^{19}F–^{13}C$ correlation NMR for ^{19}F resonance assignment of fluorinated proteins', *Journal of Biomolecular NMR*, 74(2–3), pp. 193–204. Available at: https://doi.org/10.1007/s10858-020-00306-0.

Shuwirda, B.S., Yu, G. and Mark, A. (2023) 'Chapter one - The application of the Fischer indole synthesis in medicinal chemistry', in Eric F.V. Scriven and Christopher A. Ramsden (eds.) *Advances in Heterocyclic Chemistry*, pp. 1–85. Available at: https://doi.org/10.1016/bs.aihch.2022.11.001.

Simoneau C.A. and Ganem B. (2008) “A three-component Fischer indole synthesis,” *Nature Protocols*, 3, pp. 1249–1252. Available at: https://doi.org/https://doi.org/10.1038/nprot.2008.94.

Socea, L.-I. *et al*. (2022) ‘Acylhydrazones and their biological activity: a Review’, *Molecules*, 27(24), p. 8719. Available at: https://doi.org/10.3390/molecules27248719.

Sravanthi, T.V. and Manju, S.L. (2016) ‘Indoles, a promising scaffold for drug development’, *European Journal of Pharmaceutical Sciences*, 91, pp. 1–10. Available at: https://doi.org/10.1016/j.ejps.2016.05.025.

Stoitsov, D. *et al*. (2024) ‘A complete ^{1}H and ^{13}C NMR data assignment for three 3-[Substituted methylidene]-1H,3H-naphtho-[1,8-cd]-pyran-1-ones’, *Crystals*, 14(10), p. 871. Available at: https://doi.org/10.3390/cryst14100871.

Taber, D.F. and Tirunahari, P.K. (2011) ‘Indole synthesis: a review and proposed classification’, *Tetrahedron*, 67(38), pp. 7195–7210. Available at: https://doi.org/10.1016/j.tet.2011.06.040.

Teixeira, S., Castanheira, E.M.S. and Carvalho, M.A. (2025) ‘Hydrazides as powerful tools in medicinal chemistry: synthesis, reactivity, and biological

applications', *Molecules*, 30(13), p. 2852. Available at: https://doi.org/10.3390/molecules30132852.

Tiquia-Arashiro, S. *et al*. (2023) 'Applications of fourier transform-infrared spectroscopy in microbial cell biology and environmental microbiology: advances, challenges, and future perspectives', *Frontiers in Microbiology*, 14, p. 1304081. Available at: https://doi.org/10.3389/FMICB.2023.1304081.

Ukaji, Y. and Soeta, T. (2012) '3.6 Acetogenin (Polypriopionate) derived auxiliaries: tartaric acid', *Comprehensive Chirality*, 3, pp. 176–201. Available at: https://doi.org/10.1016/B978-0-08-095167-6.00306-2.

Vigushin, D.M. *et al*. (2003) 'Pyrazino[1,2-a]indole-1,4-diones, simple analogues of gliotoxin, as selective inhibitors of geranylgeranyltransferase I', *Bioorganic & Medicinal Chemistry Letters*, 13(21), pp. 3661–3663. Available at: https://doi.org/10.1016/j.bmcl.2003.08.022.

Vlad, I.M. *et al*. (2024) 'Synthesis and characterization of N-new *N*-acyl hydrazone derivatives of carprofen as potential tuberculostatic agents', *Antibiotics*, 13(3), p. 212. Available at: https://doi.org/10.3390/antibiotics13030212.

Xue, Y. and Nestor, G. (2022) 'Determination of amide cis/trans isomers in N-acetyl-d-glucosamine: Tailored NMR Analysis of the *N*-Acetyl Group Conformation', *ChemBioChem*, 23(17). Available at: https://doi.org/10.1002/cbic.202200338.

Zhang, B. *et al*. (2022) 'Enhancement of stability and antioxidant activity of Mulberry anthocyanins through succinic acid acylation', *Food Technology and Biotechnology*, 60(3), p. 321. Available at: https://doi.org/10.17113/FTB.60.03.22.7203.

Zhang, Jianqiang *et al*. (2018) 'Synthesis and biological evaluation of indole-2-carbohydrazide derivatives as anticancer agents with anti-angiogenic and antiproliferative Activities', *ChemMedChem*, 13(12), pp. 1181–1192. Available at: https://doi.org/10.1002/cmdc.201800033.

Zhang, M. *et al.* (2017) 'Simple and efficient approach for synthesis of hydrazones from carbonyl compounds and hydrazides catalyzed by meglumine', *Synthetic Communications*, 47(2), pp. 178–187. Available at: https://doi.org/10.1080/00397911.2016.1258476.

Zhang, Y., Roder, H. and Paterson, Y. (1995) 'Rapid amide proton exchange rates in peptides and proteins measured by solvent quenching and two-dimensional

NMR', *Protein Science*, 4(4), pp. 804–814. Available at: https://doi.org/10.1002/pro.5560040420.

Zhu, H. *et al*. (2018) 'Morin as a preservative for delaying senescence of banana', *Biomolecules*, 8(3), p. 52. Available at: https://doi.org/10.3390/biom8030052.

APPENDICES

^{1}H NMR (400 MHz, DMSO-d_6) spectrum of carboxylic acid hydrazide

^{13}C NMR (100 MHz, DMSO-d_6) spectrum of carboxylic acid hydrazide

DEPT 135 spectrum of carboxylic acid hydrazide

HMQC spectrum of carboxylic acid hydrazide

HMBC spectrum of carboxylic acid hydrazide

^{1}H NMR (400 MHz, DMSO-d_6) spectrum of **SB 1**

^{13}C NMR (100 MHz, DMSO-d_6) spectrum of **SB 1**

DEPT 135 spectrum of **SB 1**

HMQC spectrum of **SB 1**

HMBC spectrum of **SB 1**

Differential NOE spectrum of **SB 1**

Differential NOE spectrum of **SB 1**

^{1}H (400 MHz, DMSO-d_6) NMR spectrum of **SB 2**

^{13}C (100 MHz, DMSO-d_6) NMR spectrum of **SB 2**

DEPT 135 spectrum of **SB 2**

HMQC spectrum **SB 2**

HMBC spectrum **SB 2**

Differential NOE spectrum of **SB 2**

Differential NOE spectrum of **SB 2**

^{1}H NMR (400 MHz, DMSO-d_6) spectrum of **SB 3**

^{13}C NMR (100 MHz, DMSO-d_6) spectrum of **SB 3**

DEPT 135 spectrum of **SB 3**

HMQC spectrum of **SB 3**

HMBC spectrum of **SB 3**

Differential NOE spectrum of **SB 3**

Differential NOE spectrum of **SB 3**

^{1}H NMR (400 MHz, DMSO-d_6) spectrum of **SB 4**

^{13}C NMR (400 MHz, DMSO-d_6) spectrum of **SB 4**

DEPT 135 spectrum of **SB 4**

HMQC spectrum of **SB 4**

HMBC spectrum of **SB 4**

Differential NOE spectrum of **SB 4**

Differential NOE spectrum of **SB 4**

^{1}H NMR (400 MHz, DMSO-d_6) spectrum of **SB 5**

^{13}C NMR (100 MHz, DMSO-d_6) spectrum of **SB 5**

DEPT 135 spectrum **SB 5**

HMQC spectrum of **SB 5**

HMBC spectrum of **SB 5**

Differential NOE spectrum of **SB 5**

Differential NOE spectrum of **SB 5**

^{1}H NMR (400 MHz, DMSO-d_6) spectrum of **SB 5**

^{13}C NMR (400 MHz, DMSO-d_6) spectrum of **SB**

DEPT 135 spectrum of **SB 6**

HMQC spectrum of **SB 6**

HMBC spectrum of **SB 6**

Differential NOE spectrum of **SB 6**

Differential NOE spectrum of **SB 6**

^{1}H NMR (400 MHz, DMSO-d_6) spectrum of **SB 7**

^{13}C NMR (100 MHz, DMSO-d_6) spectrum of **SB 7**

DEPT 135 spectrum of **SB 7**

HMQC spectrum of **SB 7**

HMBC spectrum of **SB 7**

Differential NOE spectrum of **SB 7**

\

Differential NOE spectrum of **SB 7**

^{1}H NMR (400 MHz, DMSO-d_6) spectrum of **SB 8**

^{13}C NMR (400 MHz, DMSO-d_6) spectrum of **SB 8**

DEPT 135 spectrum of **SB 8**

HMQC spectrum of **SB 8**

HMBC spectrum of **SB 8**

Differential NOE spectrum of **SB 8**

Differential NOE spectrum of **SB 8**

^{1}H NMR (400 MHz, DMSO-d_6) spectrum of **SB 9**

^{13}C NMR (100 MHz, DMSO-d_6) spectrum of **SB 9**

DEPT 135 spectrum of **SB 9**

HMQC spectrum of **SB 9**

HMBC spectrum of **SB 9**

Differential NOE spectrum of **SB 9**

Differential NOE spectrum of **SB 9**

^{1}H NMR (400 MHz, DMSO-d_6) spectrum of **SB 10**

^{13}C NMR (400 MHz, DMSO-d_6) spectrum of **SB 10**

DEPT 135 spectrum of **SB 10**

HMQC spectrum of **SB 10**

HMBC spectrum of **SB 10**

Differential NOE spectrum of **SB 10**

Differential NOE spectrum of **SB 10**